HELLENIC REPUBLIC
National and Kapodistrian
University of Athens

Department of Geology & Geoenvironment

Diploma Thesis

''Petrographic study of the hydrothermal alterations in the Piavitsa gold deposit''

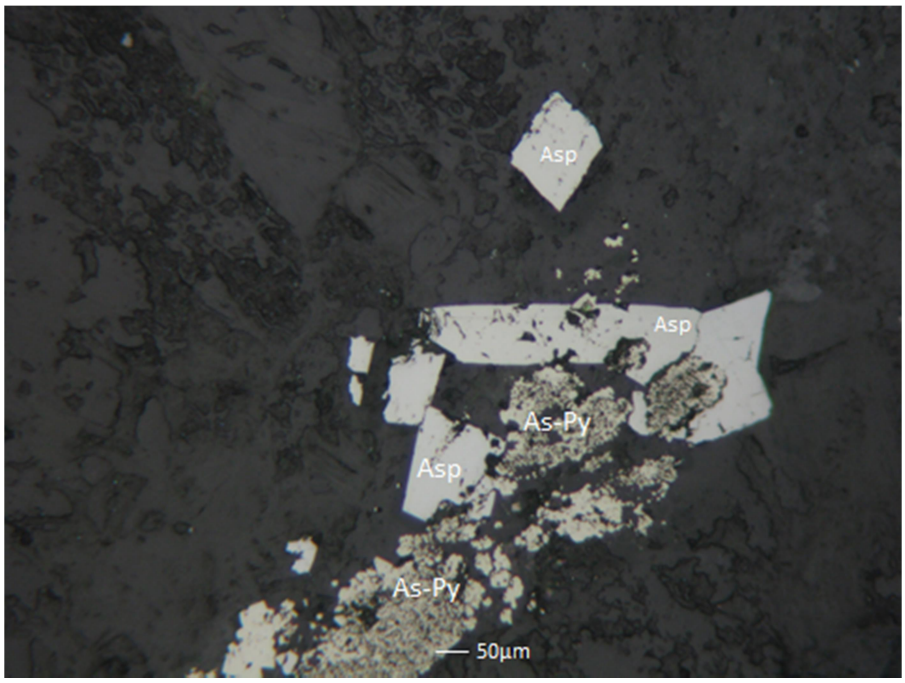

By Efkleidis Oikonomidis

Supervisor: Professor Stephanos P. Kilias

2022

Abstract

The Kassandra mining district belongs to the Serbo-Macedonian metallogenic province of the greater Tethyan mineral belt, forming a NW-trending zone of Oligo-Miocene porphyry. This zone extends from Serbia to Kassandra mining district on the eastern Chalkidiki peninsula in northern Greece (Siron et al, 2019). The Kassandra mining district belongs to the intrusion-related carbonate-hosted replacement deposit class and contains around 12 million ounces (1 ounce=28.35 grams) Au (Eldorado Gold Corp., 2016) in porphyry and carbonate-hosted replacement-style sulfide orebodies making this district one of the most economically significant mining camps in the Serbo-Macedonian metallogenic province (Siron et al, 2016).

The Stratoni fault crosscuts the Kassandra mining district from the east to the west and hosts the Madem Lakkos, Mavres Petres and the Piavitsa prospect and has diminishing Cu concentration with decreasing Pb/Zn and Ag/Au ratios from Madem Lakkos to Piavitsa (Siron et al, 2019).

Piavitsa is located in the western end of the Stratoni fault zone and hosts siliceous Mn-rich replacement bodies and contains an inferred resource of 6.613 Mt grading 4,82 g/t Au and 6.613 Mt with 54 g/t Ag (Eldorado Gold Corporation December 15, 2021).

To describe the mineral paragenesis and the mineralization style of the Piavitsa prospect as well as the reactions of the ore fluid that took place in relation with pre, main and post ore stage we used Optical Microscopy (transmitted and reflected light) and EDS-SEM analysis in order to analyze 13 samples, from seven different diamond drill holes intercepts provided by Eldorado Gold Corporation. These 13 samples are the same samples M. Tzani used in her MSc thesis in 2021, the results we found match the results of her study. Pre-ore stage is dominated by strong carbonate dissolution of primary wall-rock calcite, silicification that is accompanied by As-poor-pyrite, galena, sphalerite, chalcopyrite and Cu-Pb-Sb-sulfosalts and sulfidation. Main-ore stage is identified by the presence of presumable Au-bearing As-pyrite and arsenopyrite. Main ore stage minerals include arsenopyrite, As-pyrite, Fe-kutnohorite 1, rhodochrosite 1, kutnohorite 2, illite, rutile and apatite. Main-ore stage alterations are sulfidation, argillization, silicification, and carbonatization. Post-ore stage is characterized by rhodochrosite 2 which is the product of post-ore carbonatization.

Περίληψη

Η μεταλλευτική περιοχή της Κασσάνδρας υπάγεται στην Σερβο-Μακεδονική μεταλλευτική περιοχή της ευρύτερης ζώνης της Τηθύος, δημιουργόντας μια ΒΔ ζώνη από Ολιγο-Μειοκαινικές πορφυρικές διεισδύσεις. Αυτή η ζώνη εκτείνεται από την Σερβία μέχρι την μεταλλευτική περιοχή της Κασσάνδρας, στην Χαλκιδική, στην Β. Ελλάδα. Η μεταλλευτική περιοχή της Κασσάνδρας ανήκει σε κοιτάσματα συμπαγών θειούχων από αντικατάσταση ανθρακικών που σχετίζονται με μαγματική διείσδυση και περιέχει περίπου 12 εκατ. ουγκιές (1 ουγκια=28,35 γραμμάρια) σε πορφυρικά και συμπαγή θειούχα από αντικατάσταση ανθρακικών κάνοντας αυτήν την περιοχή την πιο οικονομικά σημαντική περιοχή στη Σερβο-Μακεδονική μεταλλογενετική περιοχή.

Το ρήγμα του Στρατωνίου τέμνει την μεταλλευτική περιοχή της Κασσάνδρας από την ανατολή προς την δύση και πάνω στο ρήγμα αυτό υπάρχουν τα μεταλλεία του Μαντέμ Λάκκου, των Μαύρων Πετρών και της Πιάβιτσας, και ελαχιστοποιούνται οι συγκεντρώσεις χαλκού καθώς μειώνεται η αναλογία Pb/Zn και Ag/Au από του Μαντέμ Λάκκου προς την Πιάβιτσα.

Η Πιάβιτσα βρίσκεται στο δυτικό άκρο του ρήγματος του Στρατωνίου, περιέχει πυριτιωμένα σώματα αντικατάστασης, πλούσια σε μαγγάνιο, και έχει 6.613 εκατ. τόνους περιεκτικότητας 4,82 γραμ./τόνο χρυσού και 6.613 εκατ. τόνους περιεκτικότητας 54 γραμ./τόνο αργύρου.

Προκειμένου να περιγράψουμε την παραγενετική ακολουθία και τον τρόπο κρυστάλλωσης στο κοίτασμα της Πιάβιτσας καθώς επίσης και τις αντιδράσεις των υδροθερμικών ρευστών, που έλαβαν μέρος σε σχέση με την απόθεση του μεταλλεύματος, χρησιμοποιήσαμε οπτικό μικροσκόπιο και EDS-SEM analysis έτσι ώστε να αναλύσουμε 13 δείγματα λεπτών τομών που προέρχονται από καρότα γεωτρήσεων από 7 διαφορετικές γεωτρήσεις.

Αυτά τα 13 δείγματα είναι τα ίδια δείγματα που χρησιμοποίησε η Μ. Τζανή στην μεταπτυχιακή της έρευνα το 2021. Τα αποτελέσματα που βρήκαμε ταιριάζουν με τα αποτελέσματα της Μ. Τζανής. Το στάδιο πριν την απόθεση του μεταλλεύματος κυριαρχείται από ισχυρή διάληση του μητρικού ασβεστιτικού πετρώματος, πυριτίωση που συνοδεύεται από φτωχό σε αρσενικό σιδηροπυρίτη, γαληνίτη, σφαλερίτη, χαλκοπυρίτη, και θειοάλατα-Cu-Pb-Sb, και σουλφιδίωση. Το κύριος στάδιο μεταλλεύματος αναγνωρίζεται από την παρουσία του αρσενούχου σιδηροπυρίτη και του αρσενοπυρίτη που πιθανώς περιέχουν χρυσό. Το κυρίως στάδιο μεταλλεύματος περιέχει αρσενοπυρίτη, αρσενούχο σιδηροπυρίτη, σιδηρούχου κουτνοχορίτη-

1, ροδοχρωσίτη-1, κουτνοχορίτη-2, ιλλίτη, ρουτίλιο και απατίτη. Το ύστερο στάδιο μεταλλεύματος χαρακτηρίζεται από την παρουσία του ροδοχρωσίτη-2 που πρόκειται για προϊόν ασβεστοποίησης.

Acknowledgments

First of all I would like to thank my supervisor professor, Stephanos P. Kilias for giving me a chance to work with him, for the amazing subject of my diploma thesis he had available for me and for all the things I learned from him. He has motivated me to take the harder path to success despite being more difficult.

Also I would like to thank my friend Vasilis Pletsas, who was extremely helpful with everything I needed.

I would like to dedicate this research to my family for the support throughout my years in the university, especially during my research time on my diploma thesis.

Table of Contents

Regional Geology of the Kassandra mining district: Vertiskos and Kerdilion units

Vertiskos unit belongs to the ‘’allochthon pre-alpine background of Rhodope’’. It hosts Variscan gneiss, migmatites and Paleozoic to Mesozoic granites while it lacks marbles. Some granite is Paleozoic, while some deep alkali-granite intrusions and migmatites are late-Jurassic. Also Triassic granites have been identified in the region of Chalkidiki. The base of this unit is manifested by metamorphic serpentine bodies which mark the lower limit of this unit. Kerdilion unit belongs to the ‘’Serbo-Macedonian unit’’ and is placed beneath Vertiskos unit. The base of Kerdilion unit hosts gneiss amphibolite and mica schist while they are crosscut by granite intrusions and pegmatite. The upper part of the unit is dominated by marbles (Dimitrios I. Papanikolaou, Geology of Greece)

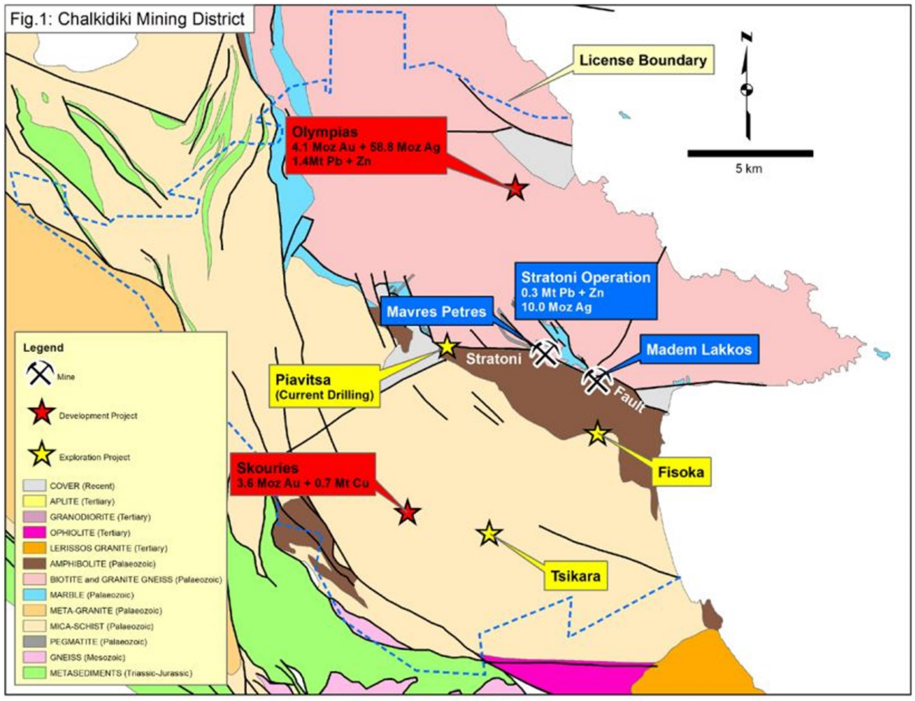

Fig. 1. Eldorado Gold Corporation, June 27, 2012. Chalkidiki Mining District.

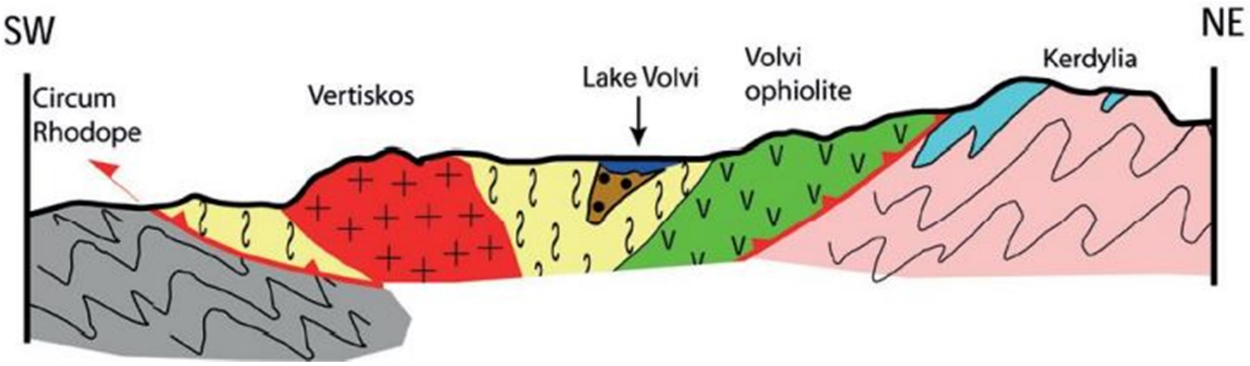

Fig. 2. Simplified geological section showing the placement of ''allochthon pre-alpine background of Rhodope'' upon ''Serbo-Macedon'' unit. Papanikolaou, 2009

Stratoni fault has brought Vertiskos and Kerdilion units together. Piavitsa prospect is located along this fault.

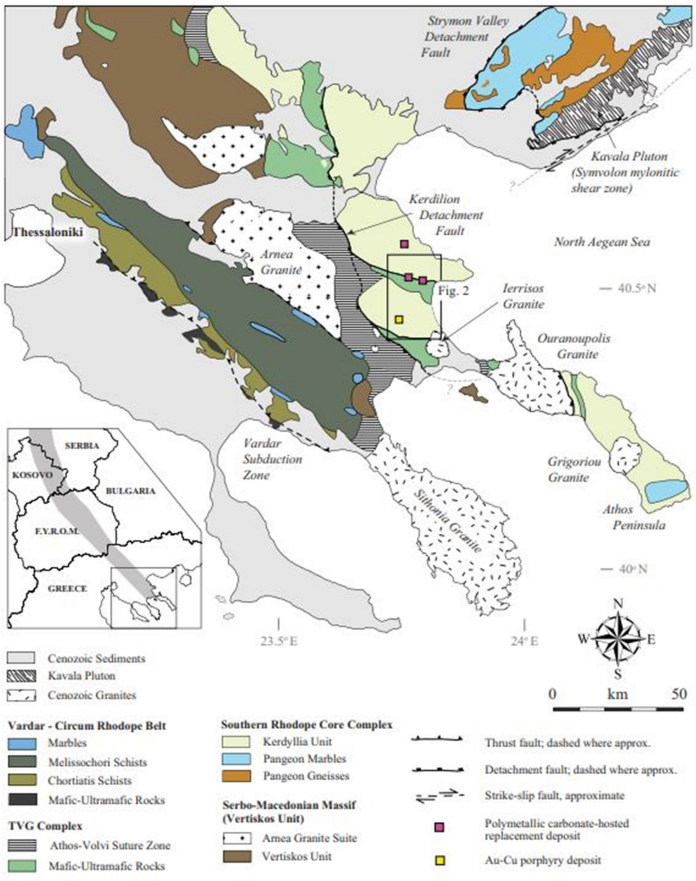

Fig. 3. Simplified geologic map of the Chalkidiki peninsula after Himmerkus et al. (2011), including the Strymon valley detachment fault adopted from Dinter (1998) and the northern segment of the Kerdilion detachment fault after Brun and Sokoutis (2007) and Wüthrich (2009). Inset map depicts the location of the Oligo-Miocene Serbo-Macedonian Lece-Chalkidiki metallogenic belt (gray) after Jankovi´c (1997) and Serafimovski (2000). (Siron et. Al., 2016 and references therein).

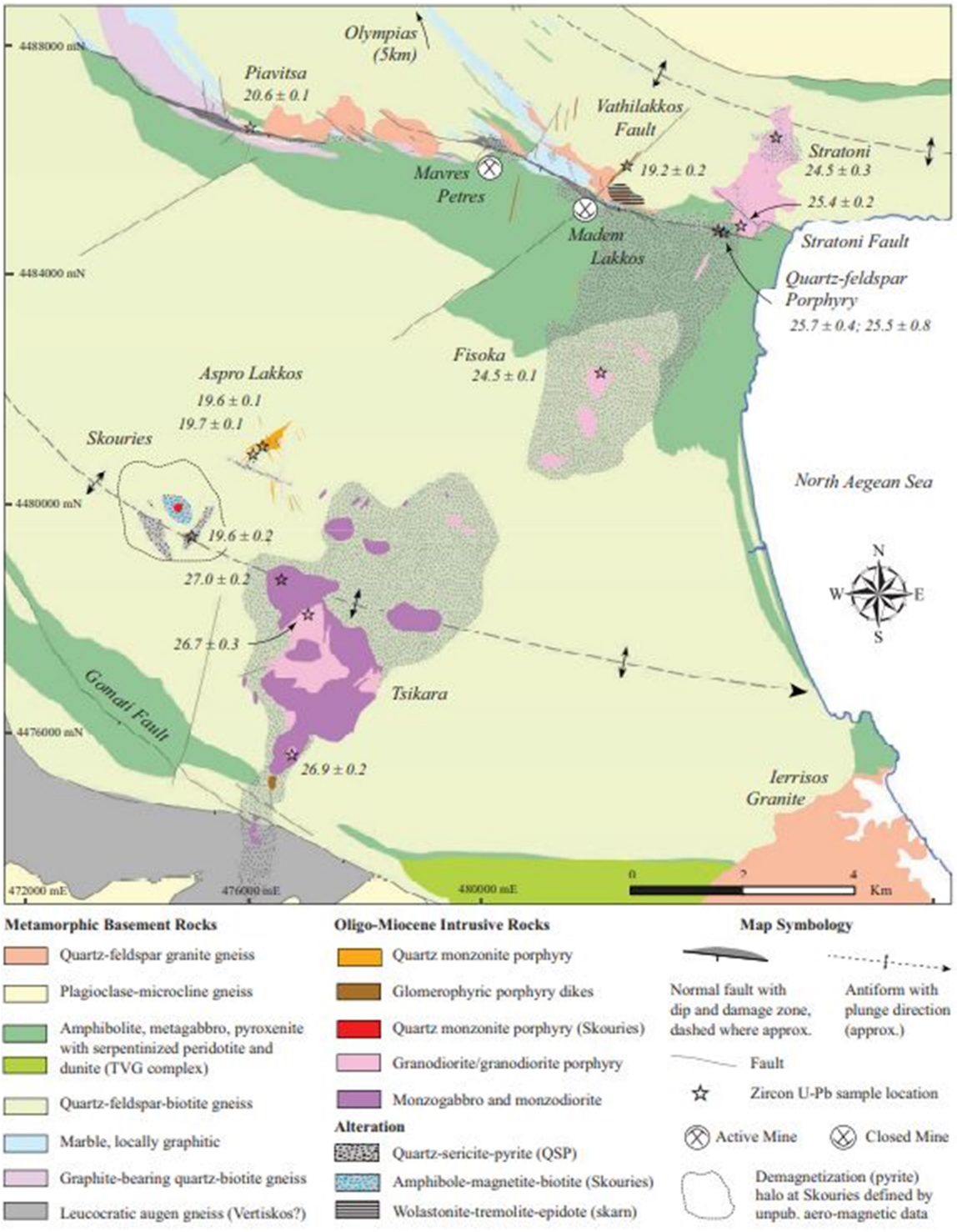

Fig. 4. Geologic map of the Kassandra mining district modified after Kockel et al. (1975). Coordinates measured using Greek Geodetic Coordinate System (GGRS 87 Greek Grid) (Siron et al., 2016).

Introduction to Carlin-type and carbonate replacement deposits

Sediment-hosted gold deposits, also known as Carlin-type gold deposits, are among the largest hydrothermal gold deposits in the world (Kesler et al., 2005). Carlin-type gold deposits are epigenetic, disseminated, auriferous pyrite (marcasite or arsenopyrite) deposits characterized by carbonate dissolution, argillic alteration, sulfidation and silicification of typically calcareous sedimentary rocks. Gold and pyrite precipitate together from H_2S-rich fluids by sulfidation of host-rock Fe. As a result, Fe is relatively immobile and S and Au are introduced along with trace elements, such as As, Sb, Tl, Hg, Ag, ±W, and ±Te (Hofstra & Cline, 2000). These deposits were first recognized as a new class of deposit following the discovery of Carlin in the mid 1960s (Cline, 2001). Since then, more than 1,000 tonnes of gold has been produced (Christensen, 1995) from more than 100 Carlin-type gold deposits in Nevada. Carlin-type gold deposits are also located in the Dian-Qian-Gui ''Golden Triangle'' area of the southwest China and has the second largest concentration of Carlin-type gold deposits in the world, containing more than 800 tonnes of gold (Su et al, 2018).

Carbonate-replacement deposits are part of a family of deposits zoned around magmatic-hydrothermal, intrusion centered systems that include porphyry, skarn, and vein deposits (Sillitoe, 1991a). Carbonate-replacement deposits occur as replacement-style mineralization in limestone and dolostone. They are structurally and lithologically controlled preferring permeable limestone beds, and normally occur in manto, lens and chimney-shaped bodies. Although typically mined for base metals, some carbonate-replacement deposits are Au rich and possess only minor base metal enrichment (Albino, 1995). Sillitoe and Bonham (1990) proposed that Au-rich carbonatereplacement deposits form the most distal member of the sequence of intrusion-related deposits in zoned intrusioncentered camps. The dominant sulfide mineral assemblage in Au-rich carbonate-replacement deposits consist of pyrite, arsenopyrite, sphalerite, galena, chalcopyrite, marcasite, and pyrrhotite, and their geochemical signature, which is more variable than in Carlin-type deposits, consists of As-Sb-Pb-Zn ± Ag, Mn, Tl, Te, Cu, Hg, Bi, and Sn (Thompson 2004).

Piavitsa prospect of the Kassandra mining district

The Piavitsa prospect is a gold-silver rich, polymetallic carbonate replacement prospect similar to the Olympias deposit. It is localized along the Stratoni Fault, approximately 4 km to the west of the Mavres Petres deposit which is presently being mined at the Stratoni Mine. The prospect was previously mined in the 1960s in shallow pits for manganese oxide by the Hellenic Fertilizer Company SA. Exploration during this era included 47 drillholes testing shallow targets along the Stratoni. Although many of these historic drillholes intersected massive sulphide intervals, they were not assayed for gold and silver. In 1998, TVX completed an additional nine drillholes, mostly targeting the central and eastern portions of the prospect. Grades in these drillholes (as previously reported by European Goldfields) included intervals of 10.9 m @ 7.88 g/t Au and 199.04 g/t Ag, 12 m @ 7.44 g/t Au and 107.84 g/t Ag and 8 m @ 8.64 g/t Au and 196.48 g/t Ag. Mapping and sampling programs completed in 2011 documented the distribution of manganese oxide zones, mining excavations and high gold grades in outcrops over a strike length of 3 km at Piavitsa. Airborne geophysical surveys (EM, magnetics) show a strong anomaly associated with the known mineralized zone which has an east-west strike extended to over 8 km (Fig. 4, Fig. 5) (Eldorado Gold Corporation, June 27, 2012).

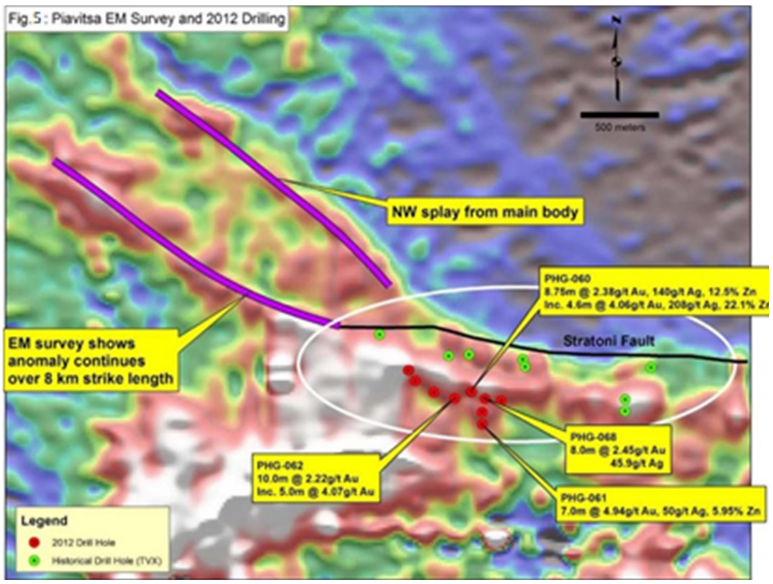

Fig. 5. Piavitsa EM Survey and 2012 Drilling (Eldorado Gold Corp., 2012).

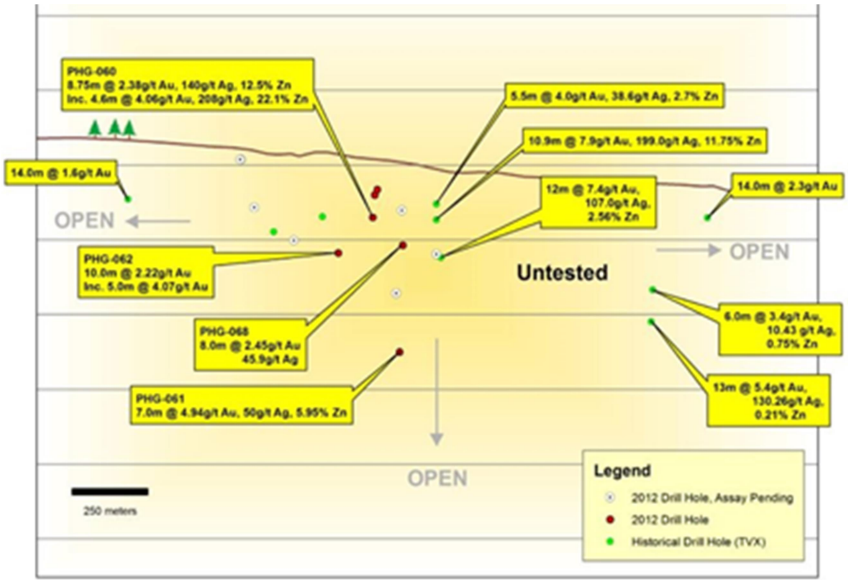

Fig. 6. Piavitsa Drilling, Inclined Longitudinal Section (Eldorado Gold Corp., 2012).

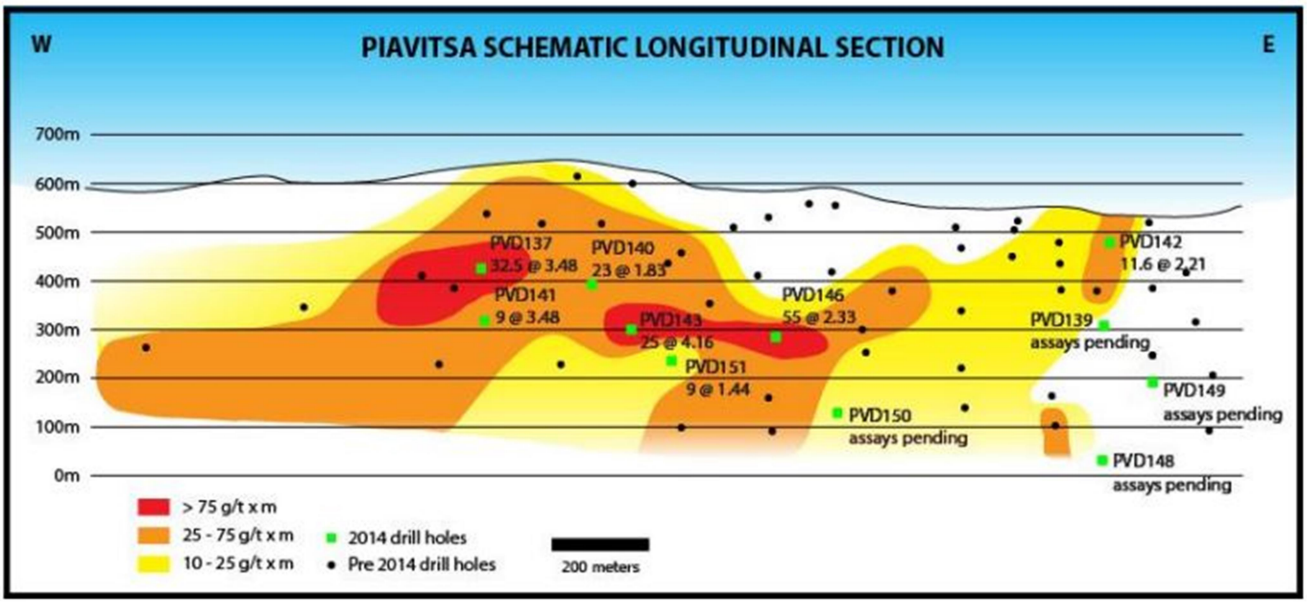

Fig. 7. Piavitsa Schematic Longitudinal Section, showing drillhole grade x thickness contours and piercing points of reported mineralized intersections and previous drillholes. (Eldorado Gold Corp., 2014).

As of September 30, 2021 Eldorado Gold Corporation has published the inferred resources of Piavitsa prospect totaling 6.613 Mt with 4,82 g/t Au, (1,025 Moz Au) with cut-off grade 4,0 g/t Au and 6.613 Mt with 54 g/t Ag, (11,389 Moz Ag) (Eldorado Gold Releases Update Mineral Reserve and Mineral Resources Statement, December 15, 2021).

Introduction

Marina Tzani in her M.Sc. thesis in 2021 analyzed with EDS-SEM analysis 13 samples. In this diploma thesis we took the same 13 samples M. Tzani used and analyzed them using Optical Microscopy in both transmitted and reflected light. The results of this thesis match the results of M. Tzani thesis.

Statement of the Problem-Scope of Thesis-Research Hypothesis

The problem-scope of this thesis is to identify and order the minerals in the different ore stages in relation to the ore-bearing As-pyrite and arsenopyrite, using Optical Microscopy (transmitted and reflected light) and EDS-SEM analysis, and to describe the ore fluid reactions that accompanied the formation of this minerals (e.g. sulfidation, decarbonatization).

Materials and Analytical Methods

Sampling

The drill core material we used in this diploma thesis was provided by Eldorado Gold Corporation (Hellas Gold S.A., Kassandra mines, Chalkidiki, N. Greece) and was carried out in Piavitsa prospect along Stratoni fault. In total we were provided with 57 samples from 7 different drilling holes.

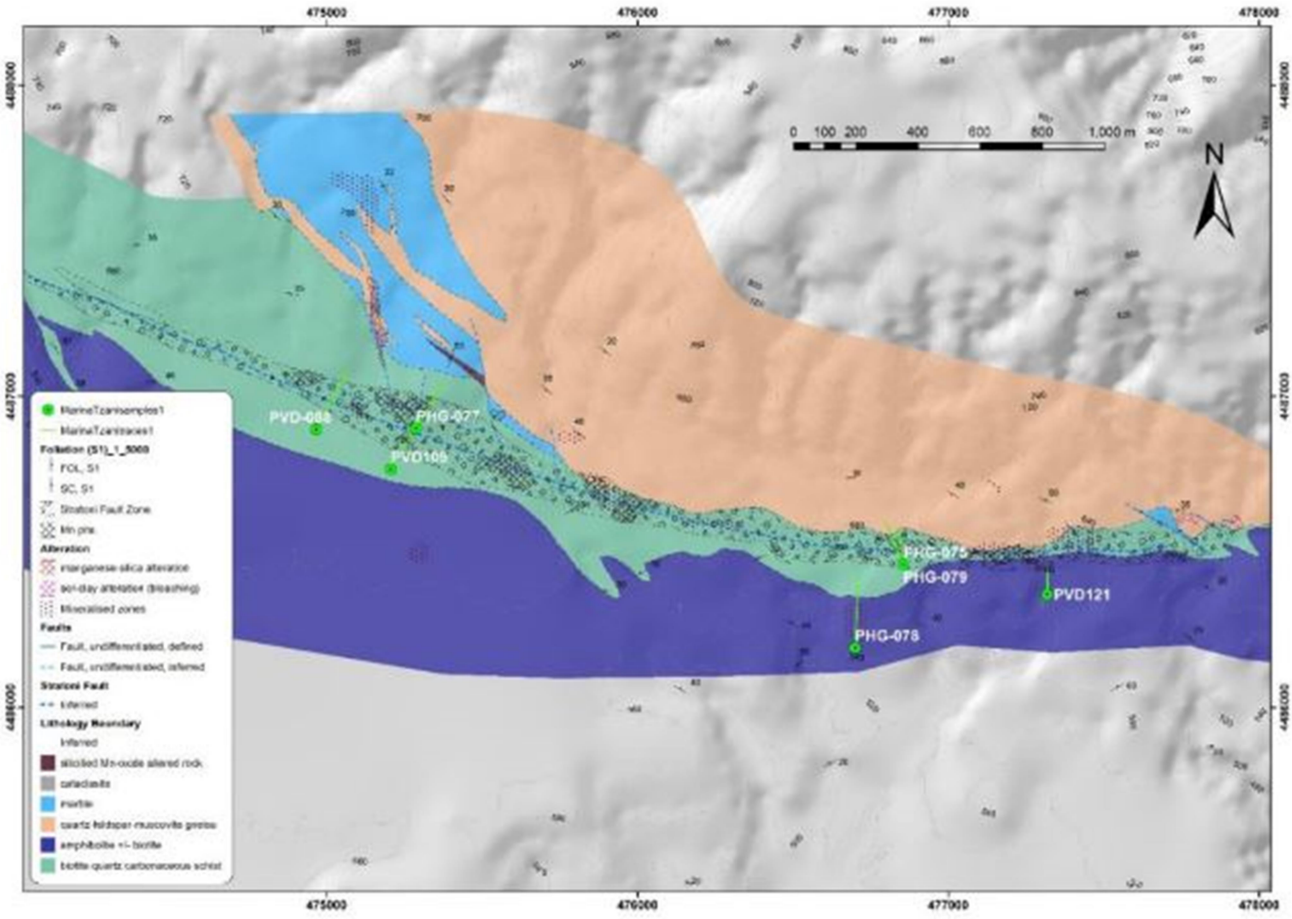

Fig. 8. Simplified geological map of the study area – Piavitsa prospect. Sample location is displayed.

(Eldorado gold Corp., 2018)

The logging of the collected sample from the drill holes:

Hole ID	Samples ID	Depth (m)	Logging
PVD-088	PI-18-1	118	Brecciated Rock Mn - rich
PVD-088	PI-18-2	117	Brecciated Rock Mn - rich
PVD-088	PI-18-3	116	Altered Schist
PVD-088	PI-18-4	115	Brecciated Rock Mn - rich
PVD-088	PI-18-5	110	Altered Schist
PVD-088	PI-18-6	101	Brecciated Rock Mn - rich
PVD-088	PI-18-7	104	Brecciated Rock Mn - rich
PVD-088	PI-18-8	100	Brecciated Rock Mn - rich
PHG-078	PI-18-9	87	Ampibolite
PHG-078	PI-18-10	90	Ampibolite

PHG-078	PI-18-11	91	Ampibolite
PHG-078	PI-18-12	96	Ampibolite
PHG-078	PI-18-13	98	Brecciated Rock Mn - rich
PHG-078	PI-18-14	102	Ampibolite
PHG-078	PI-18-15	100	Brecciated Rock Mn - rich
PHG-078	PI-18-16	107	Ampibolite
PHG-078	PI-18-17	110,8	Ampibolite
PHG-078	PI-18-18	140	Ampibolite
PHG-078	PI-18-19	144	Ampibolite
PHG-078	PI-18-20	145	Ampibolite
PHG-078	PI-18-21	146	Brecciated Rock Mn - rich
PHG-078	PI-18-22	149	Brecciated Rock Mn - rich
PHG-078	PI-18-23	154	Brecciated Rock Mn - rich
PHG-078	PI-18-24	158	Brecciated Rock Mn - rich
PHG-078	PI-18-25	269	Altered Schist
PHG-077	PI-18-26	202,5	Oxidised Marble - Mn
PHG-077	PI-18-27	203	Oxidised Marble - Mn
PHG-077	PI-18-28	204	Oxidised Marble - Mn
PHG-077	PI-18-29	204	Oxidised Marble - Mn
PHG-077	PI-18-30	206	Oxidised Marble - Mn
PHG-075	PI-18-31	34	Brecciated Rock Mn - rich
PHG-075	PI-18-32	36	Brecciated Rock Mn - rich
PHG-075	PI-18-33	37	Brecciated Rock Mn - rich
PHG-075	PI-18-34	37,8	Brecciated Rock Mn - rich
PHG-075	PI-18-35	38	Brecciated Rock Mn - rich
PHG-075	PI-18-36	42	Brecciated Rock Mn - rich
PHG-079	PI-18-37	33	Brecciated Rock Mn - rich
PHG-079	PI-18-38	35	Brecciated Rock Mn - rich
PHG-079	PI-18-39	38	Brecciated Rock Mn - rich
PHG-079	PI-18-40	41,3	Brecciated Rock Mn - rich
PHG-079	PI-18-41	44,4	Brecciated Rock Mn - rich
PVD-121	PI-18-42	57	Siliceous Mn-rich bodies
PVD-121	PI-18-43	61,8	Siliceous Mn-rich bodies
PVD-121	PI-18-44	65,1	Altered Schist
PVD-121	PI-18-45	67	Siliceous Mn-rich bodies
PVD-121	PI-18-46	68,2	Siliceous Mn-rich bodies
PVD-121	PI-18-47	71	Altered Schist
PVD-121	PI-18-49	75	Altered Schist
PVD-121	PI-18-50	73,3	Altered Schist
PVD-109	PI-18-51	120,5	Altered Schist
PVD-109	PI-18-52	124,3	Siliceous Mn-rich bodies
PVD-109	PI-18-53	133	Siliceous Mn-rich bodies
PVD-109	PI-18-54	133,9	Siliceous Mn-rich bodies

PVD-109	PI-18-55	135	Siliceous Mn-rich bodies
PVD-109	PI-18-56	137	Siliceous Mn-rich bodies
PVD-109	PI-18-57	138,5	Siliceous Mn-rich bodies
PVD-109	PI-18-58	139,5	Siliceous Mn-rich bodies

Sample Preparations

After logging, 13 samples of siliceous – manganese mineralization were selected to be studied for mineralogical analyses and thin sections were prepared at the Hellenic Survey of Geology and Mineral Exploration (M.Sc. M. Tzani, 2021). The 13 samples of siliceous-manganese mineralization we studied in this thesis are: PI-18-(11-12-13-14-16-23-25-28-31-32-39-43-58).

The samples used in this study were originated from the M.Sc. of Marina Tzani in 2021.

Analytical Methods

In order to analyze the 13 samples we used Optical Microscopy (transmitted and reflected light) and EDS-SEM analysis.

Results

Pre-Ore Minerals

Pre-ore minerals include primary host-rock (Mn-Fe)-Mg calcite, jasperoid and euhedral quartz, galena, As-poor-pyrite (hereafter pyrite), sphalerite, Cu-Pb-Sb-sulfosalts, chalcopyrite and Fe-oxides.

(Mn-Fe)-Mg calcite has a rhombohedral shape, diagonal twinning and has develop local porosity due to the decarbonatization (carbonate dissolution) of the wall rock marble (Figure 9. A, B and C, D pictures respectively).

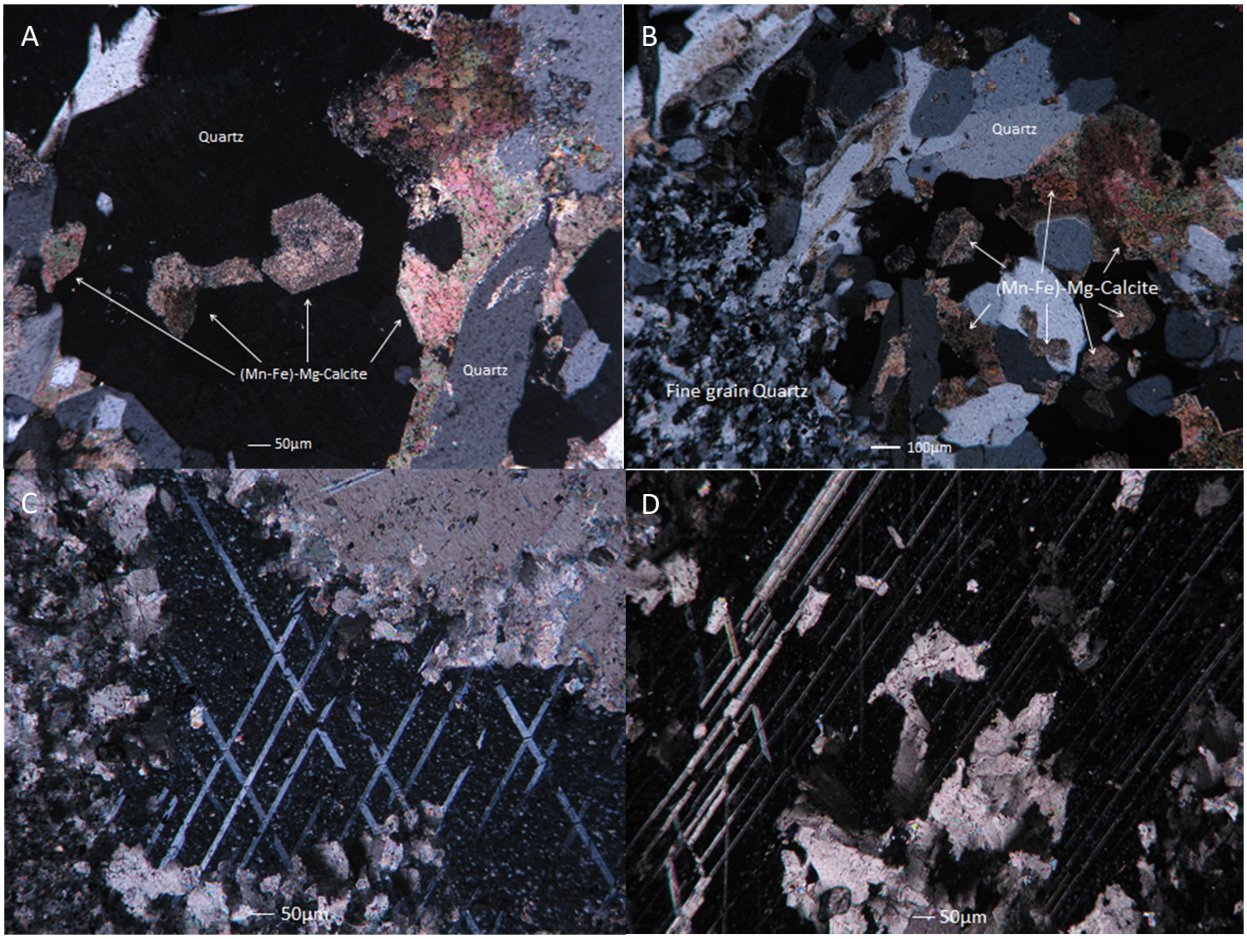

Fig. 9. Optical microscopy, transmitted light.
A-B. Primary rhomboidal (Mn-Fe)-Mg calcite in quartz.
C-D. Primary (Mn-Fe)-Mg calcite with diagonal twinning and local porosity.

More proof of the decarbonatization is the release of Fe^{2+} from the primary host-rock (Mn-Fe)-Mg calcite during decarbonatization to form Fe-oxides (Fe_2O_3) as shown in Figures 10 and 11. Strong carbonate dissolution is related with higher gold grades (Stenger et al, 1998).

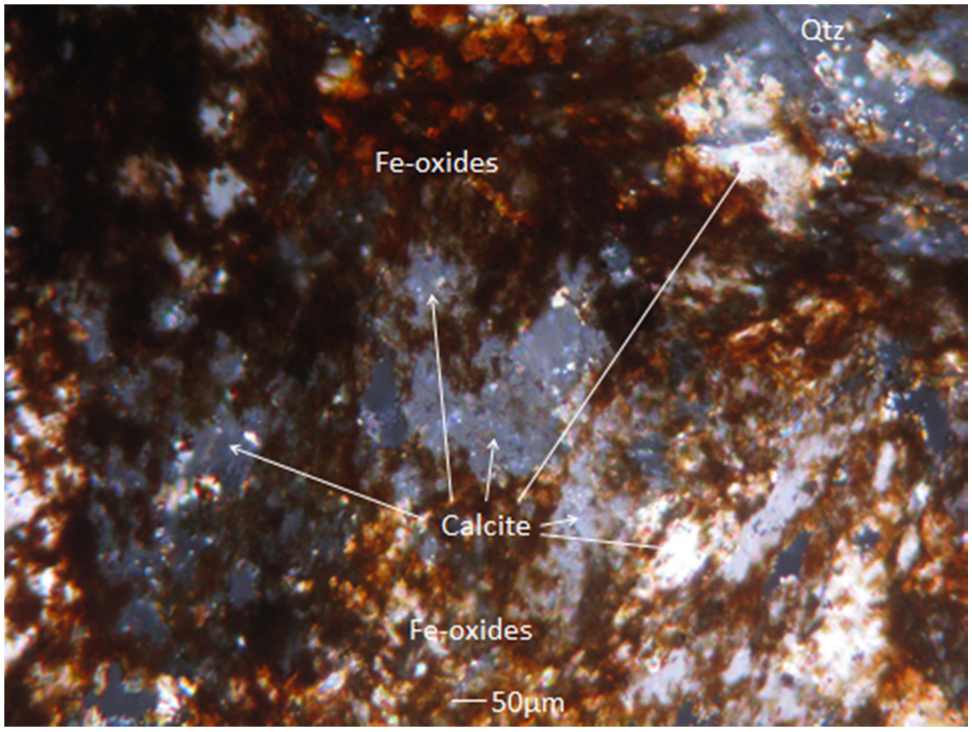

Fig. 10. Qtz=Quartz. Carbonate dissolution product (Fe-oxides) and primary calcite and quartz. Optical microscopy, transmitted light.

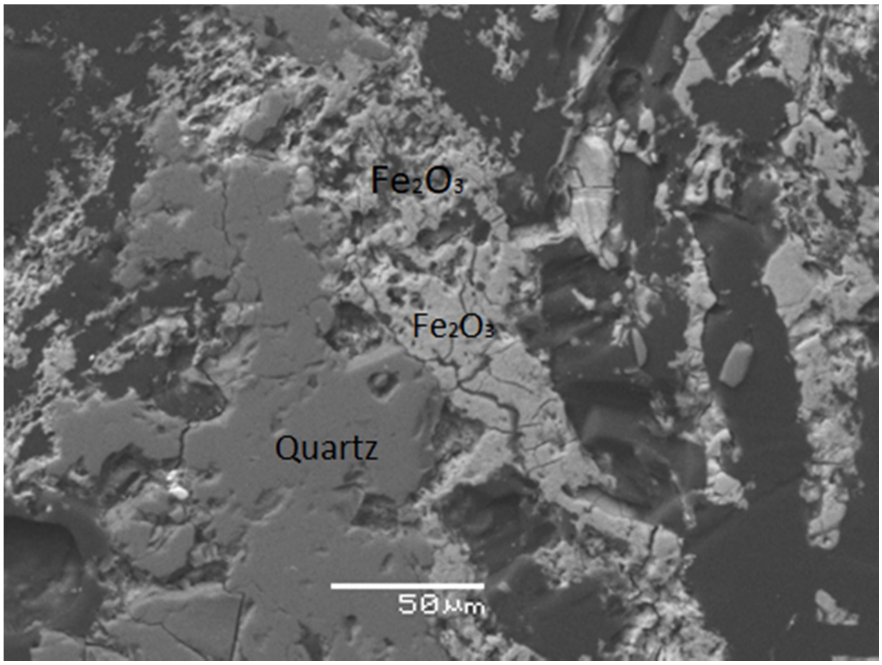

Fig. 11. Fe-oxides and quartz. EDS-SEM analysis.

Jasperoid quartz and euhedral quartz are products of the pre-ore silicification and reflect two different silicification phases. Euhedral quartz has (Mn-Fe)-Mg calcite inclusions as shown in Figures 12 and 15, indicating that quartz has replaced primary (Mn-Fe)-Mg calcite (Putnis 2002).

The second phase of silicification is fine grained vuggy jasperoid quartz with micro-calcite inclusions accompanied by pre-ore stage pyrite veins, crosscutting the already deposited euhedral quartz and primary wall rock calcite in pre-ore stage (Figure 13). Euhedral quartz is characterized by a rhombohedral shape. Both fine-grained jasperoid quartz (hereafter quartz) and euhedral quartz are inclusion rich.

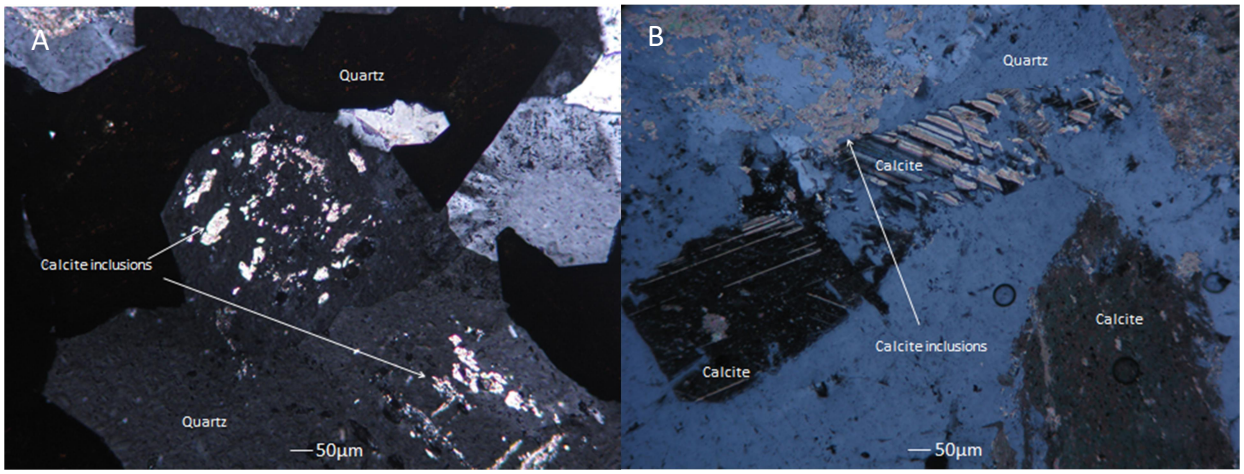

Fig. 12. Optical microscopy, transmitted light imagies. A: Quartz with micro-calcite inclusions indicating the advanced replacement of calcite by quartz. B: Calcite and quartz with calcite inclusions, the presence of primary calcite and calcite inclusions indicates weak replacement of calcite by quartz.

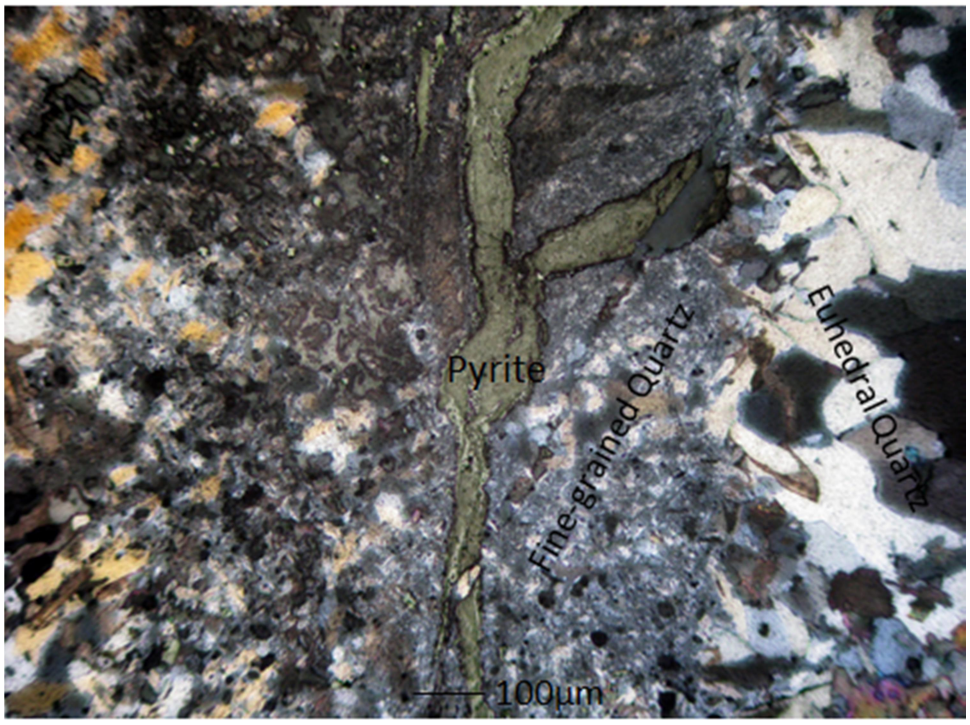

Fig. 13. Fine grained quartz accompanied by pre-ore stage pyrite vein crosscuting euhedral quartz. Optical microscopy, reflected light.

Pre-ore silicification concentrates pyrite and minor galena, sphalerite, (Figure 14). Pyrite appears in many sizes from a few mμ up to 1mm and from euhedral to subhedral when disseminated, accompanied by inclusion-rich quartz as shown in Figure 15. Pyrite also occurs in veins, while galena and sphalerite are limited to small grains either accompanying pyrite grains and veins or being dispersed within quartz.

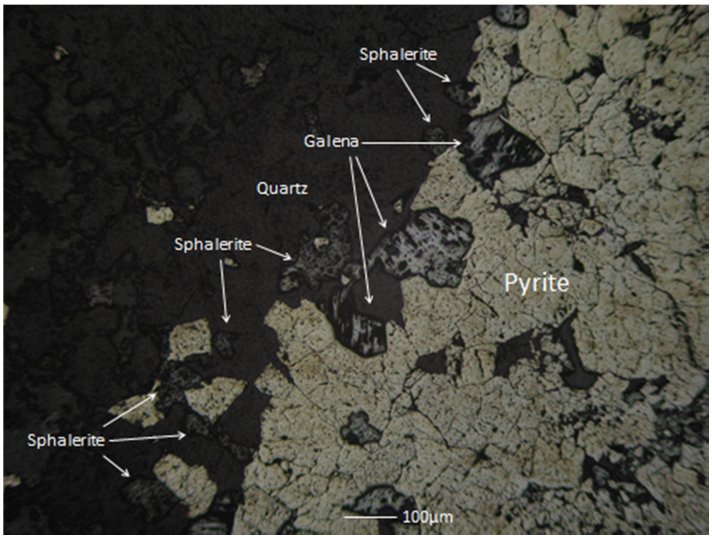

Fig. 14. Pyrite, galena, and sphalerite in inclusion-rich-quartz matrix. Optical microscopy reflected light.

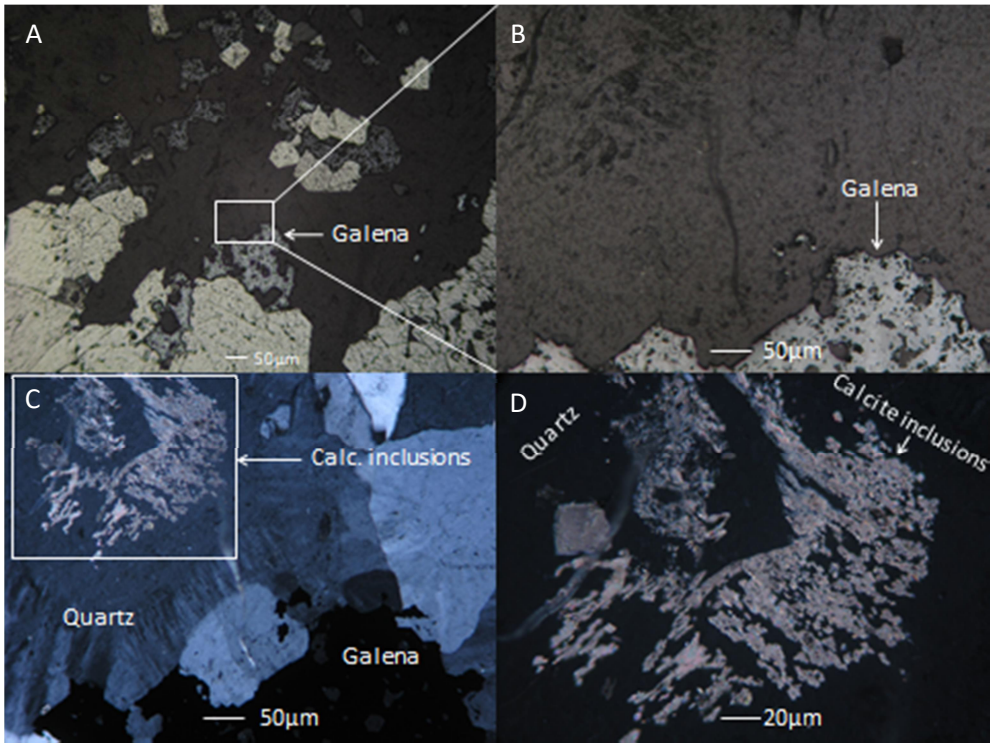

Fig. 15. A-B-C-D: Pictures of silicification in different magnitude, in both reflected and transmitted light.

Pyrite alone in quartz veins has a framboidal-like texture, a fine grained pyrite 1 partly overgrowth and outlined by euhedral pyrite 2. Euhedral pyrite 2 is associated with galena and sphalerite. Experimental studies have shown that low-temperature (<150^{o}C) pyrites that form rapidly are more likely to be fine grained and framboidal in shape compared to pyrite crystals that formed more slowly and at a higher temperature (>200^{o}C) from hydrothermal fluids or metamorphic fluids (Butler and Rickard, 2000).

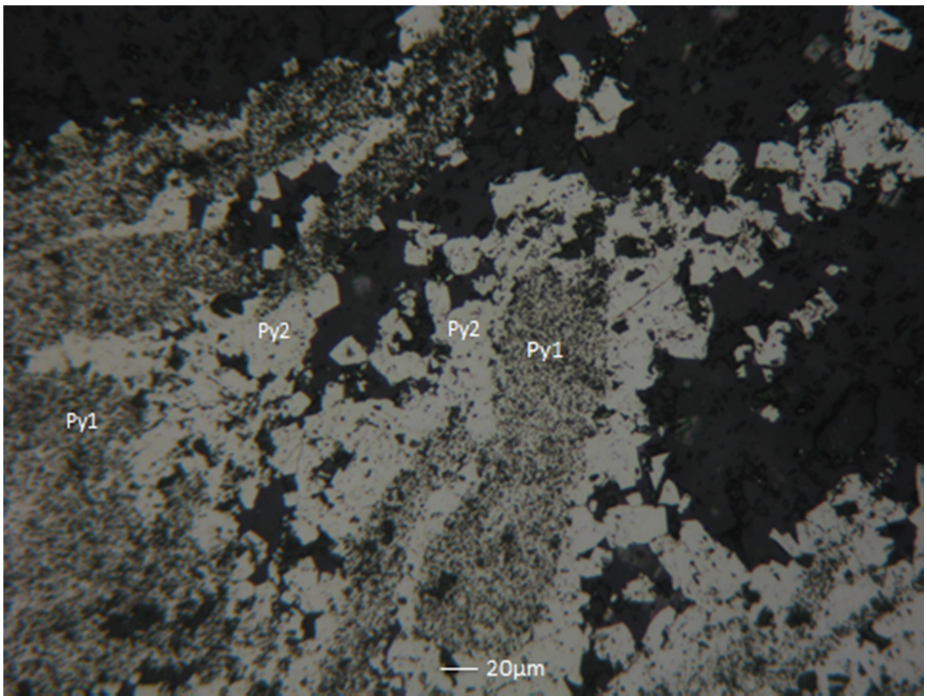

Fig. 16. Framboidal-like texture of pre-ore pyrite. Early diagenetic fine grained pyrite 1 partly overgrowth by euhedral pyrite 2. Optical microscopy, reflected light.

Also pyrite appears to be spatially associated with Fe_2O_3 (decarbonatization product) and (Mn-Fe)-Mg calcite and has (Mn-Fe)-Mg calcite inclusions, indicating the replacement of (Mn-Fe)-Mg calcite by pyrite (Putnis, 2002), during pre-ore sulfidation, as shown in Figure 17, (Hofstra & Cline, 2000).

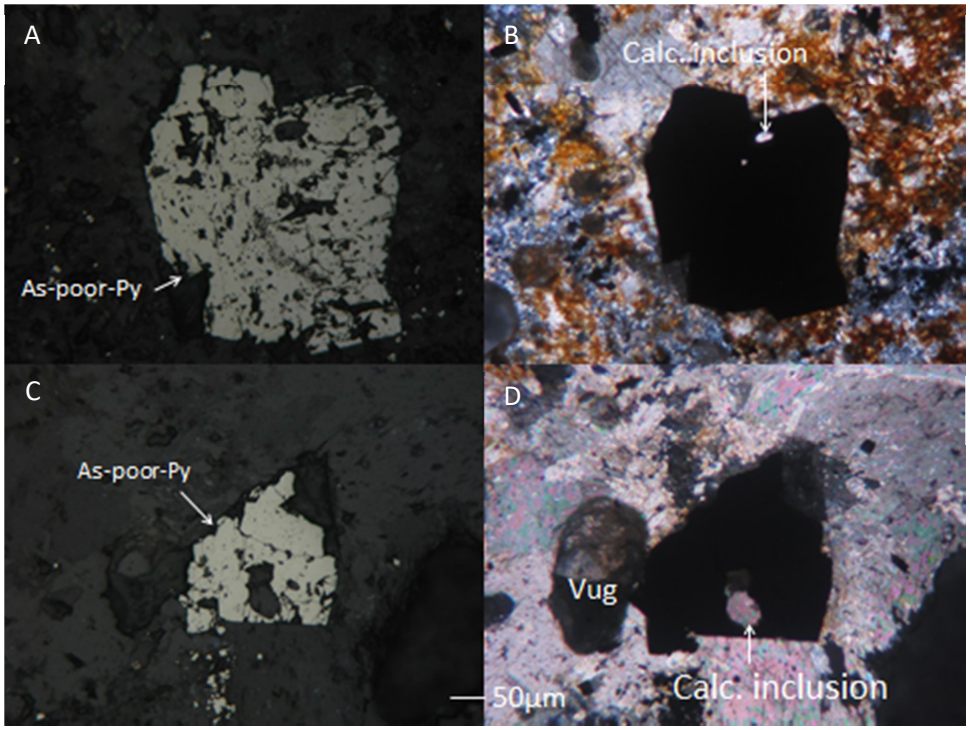

Fig. 17. Pyrite grains with calcite inclusion surrounded by calcite and Fe-oxides. Vug is a result of decarbonatization of calcite. A-C, Optical microscopy reflected light and B-D, transmitted light.

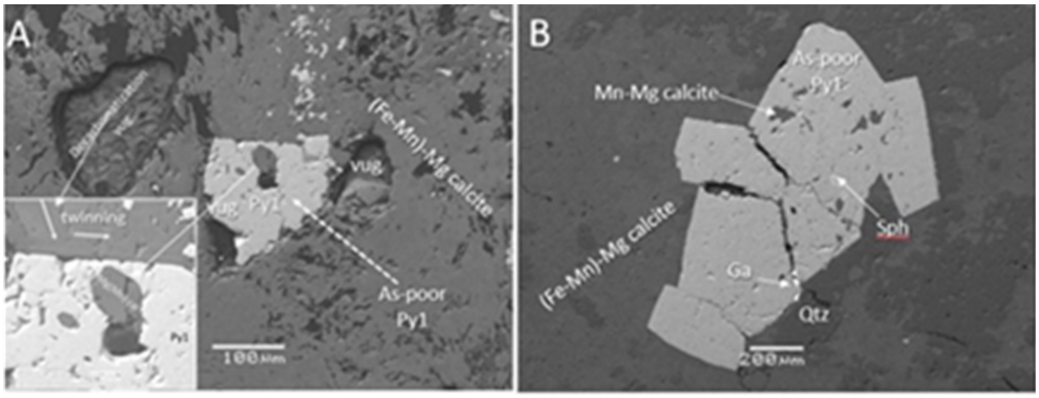

Fig. 18. EDS-SEM pictures and description from Marina Tzani M. Sc. thesis, for comparison.

A: Large, subhedral, vug-infilling As-poor pyrite 1 with Mn-Mg-calcite inclusions within vuggy decarbonatized ferrous (Mn)-Mg-rich calcite in the marble wall rock. Calcite inclusions indicate replacement of calcite by pyrite 1. Note calcite rhombohedral shape and twinning (white arrows) (inset). Note the production of enhanced secondary porosity and permeability due to decarbonatization. (M.Sc. M. Tzani 2021).

B: Assemblage of large euhedral to subhedral As-poor pyrite 1, associated with sphalerite and galena. Pyrite 1 is concentrated on jasperoid quartz that contains small relict inclusions of calcite indicating replacement of calcite by quartz.

Euhedral pyrite 1 grains contain manganiferous Mgcalcite relict inclusions also indicating replacement of calcite. Note sphalerite inclusions in pyrite 1 and galena along quartz veinlets in crosscutting pyrite. (M.Sc. M. Tzani 2021).

Minor Cu-Pb-Sb-Sulfosalts appear to rim pre-ore pyrite

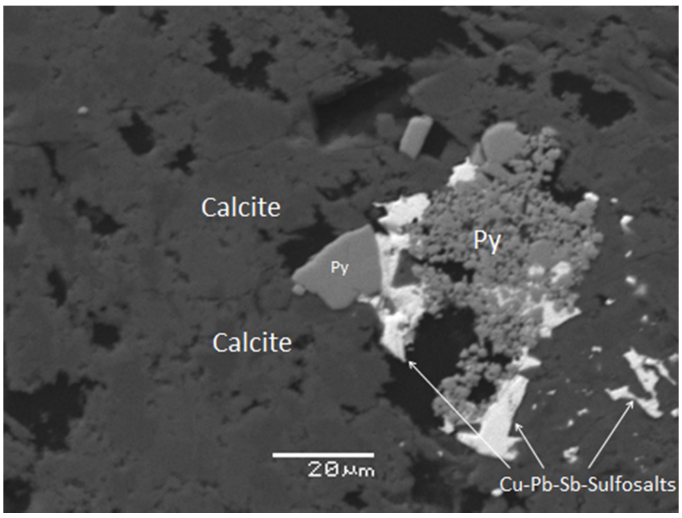

Fig. 19. Py=pyrite. Pyrite and sulfosalts hosted in calcite. EDS-SEM analysis.

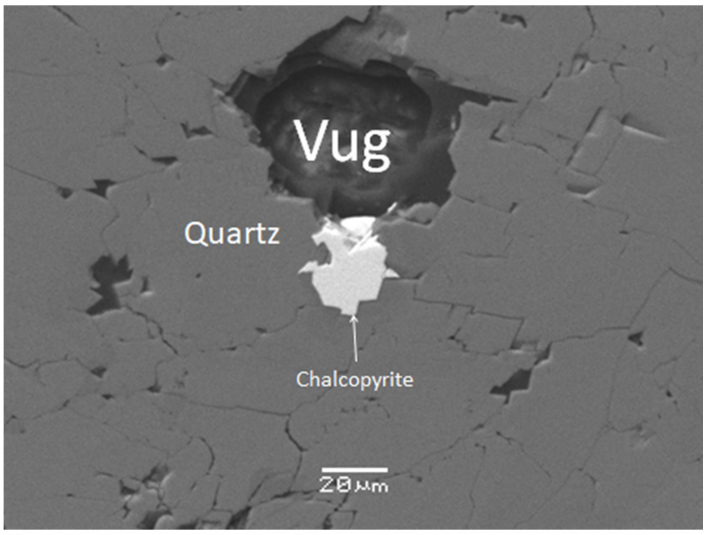

Fig. 20. Minor chalcopyrite surrounded by quartz. Vugs within quartz have irregular boundaries and edges presumably due to the toughness of quartz, while decarbonatization vugs within calcite are rounded with regular boundaries (See figure 17, picture D). EDS-SEM analysis.

Main-ore Minerals

The main ore stage is dominated by fluid-rock reactions characterized by carbonate dissolution, argillization of silicates, sulfidation of iron-bearing minerals, and silicification of limestone, that

cool and neutralize the ore fluid (Hofstra & Cline, 2000). Main ore minerals include arsenopyrite, As-pyrite, Fe-kutnohorite 1, rhodochrosite 1, kutnohorite 2, illite, rutile and apatite.

Arsenopyrite is mostly euhedral and ranges from a few µm up to 400µm. Arsenopyrite can occur either as dispersed square and rhombohedral single crystals, or they are concentrated in small clusters of several intergrown individuals. As-Pyrite commonly occurs in small veins crosscutting Arsenopyrite indicating the replacement of Arsenopyrite by As-Pyrite during main-ore stage sulfidation (Figure 21, A-B). As-pyrite alone also occurs in dispersed grains and small veins within illite and quartz matrix, (Figures 24 picture B and 25).

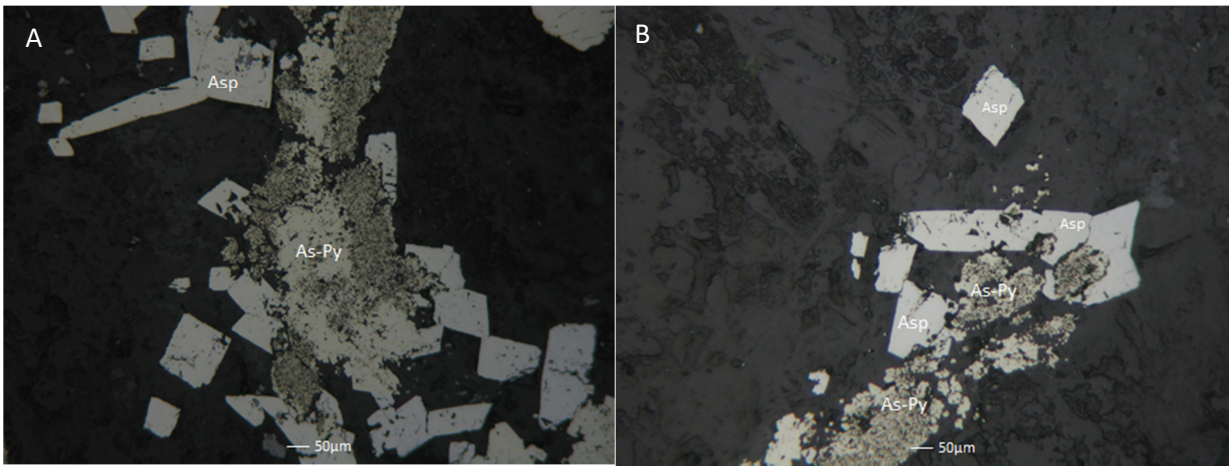

Fig. 21. Asp=Arsenopyrite, As-Py=As-Pyrite. A-B: Arsenopyrite being replaced by As-pyrite vein during main-ore stage sulfidation. Optical microscopy, reflected light.

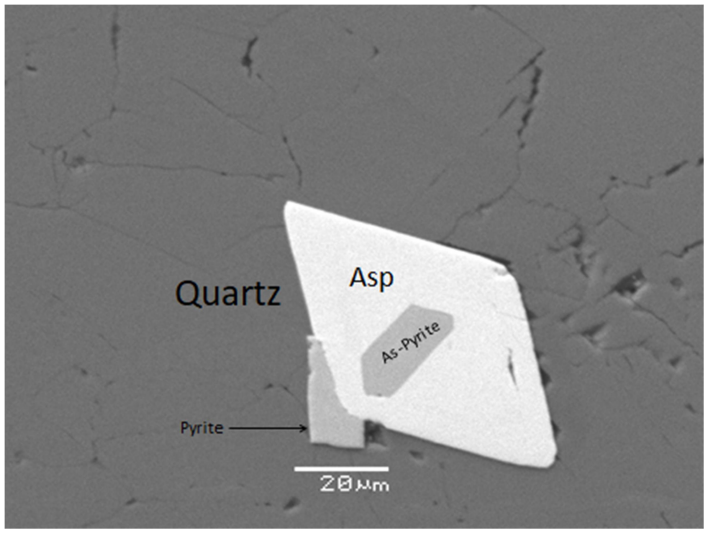

Fig. 22. Asp=Arsenopyrite. Inclusion-free-quartz surrounding rhombohedral arsenopyrite grain with As-pyrite inclusion, and pyrite. EDS-SEM analysis.

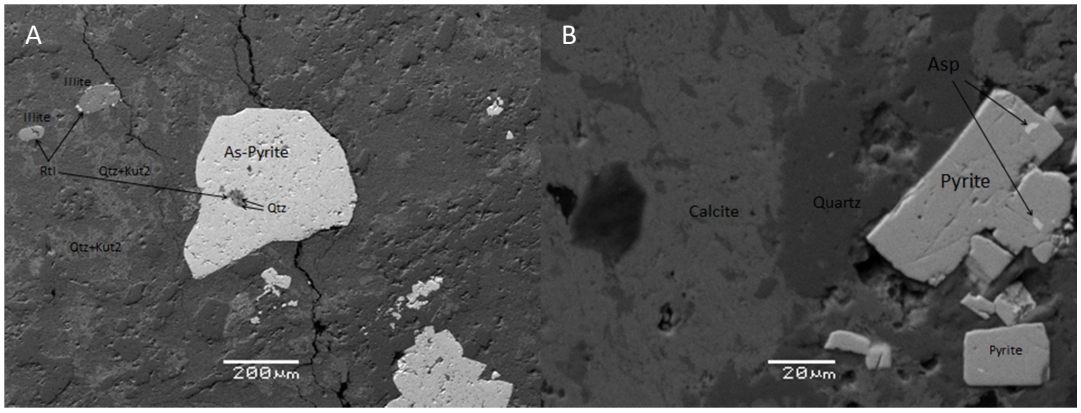

Fig. 23. Rtl=Rutile, Qtz=quartz, Kut2=Kutnohorite 2, Asp=Arsenopyrite. A: Main ore stage As-pyrite encapsulating rutile and quartz, surrounded by quartz with kutnohorite 2 inclusions and illite. EDS-SEM analysis.
B: Pyrite with arsenopyrite inclusions surrounded by quartz and calcite. EDS-SEM analysis.

Illite patches finely dispersed within the siliceous matrix suggest Illite depositions, i.e., argillization during silicification (M.Sc. M. Tzani, 2021).

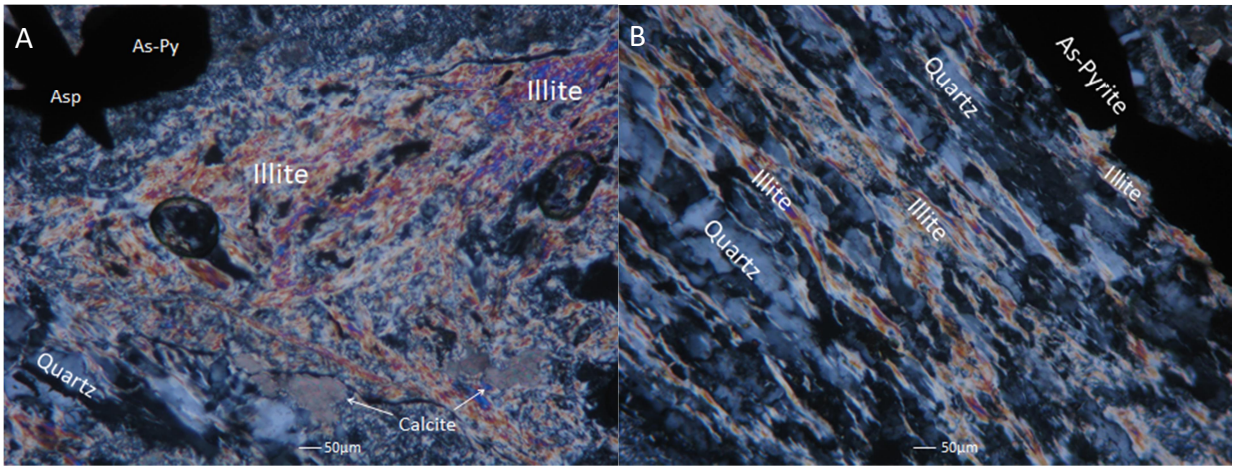

Fig. 24. Asp=arsenopyrite, As-Py= As-pyrite. A: Illite and quartz and calcite. Optical microscopy, transmitted light. B: Illite and inclusion-free-quartz accompanying As-pyrite. Optical microscopy, transmitted light.

Illite is abundant in high-grade ore (Xie et al., 2016), has pervasive texture and often accompanies arsenopyrite and As-pyrite with quartz (Figures 24 and 25).

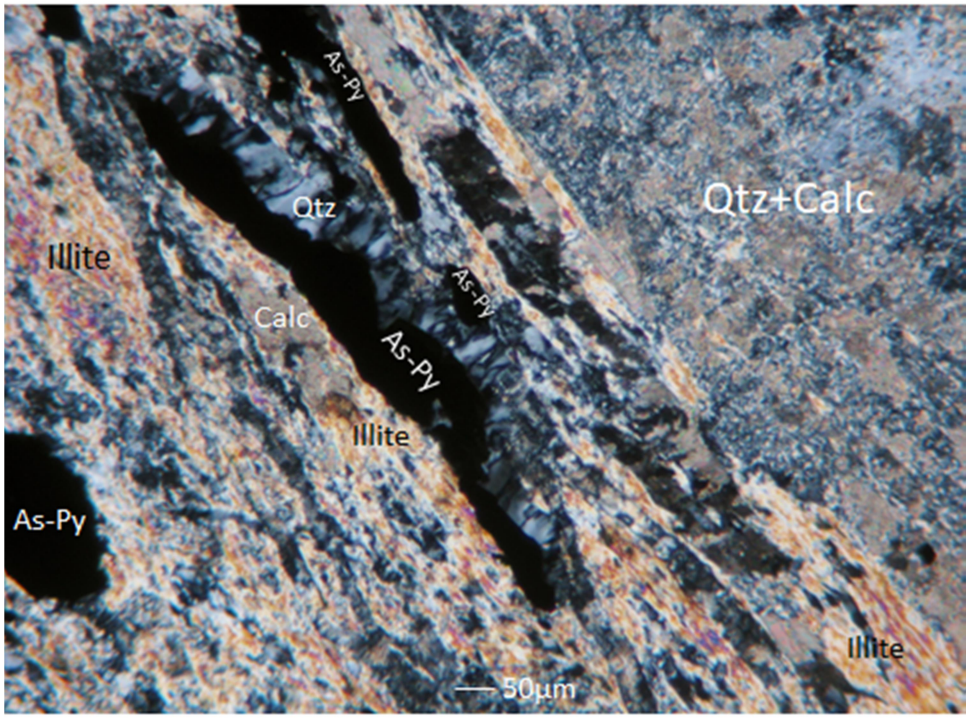

Fig. 25. As-Py=As-pyrite. Main-ore stage As-pyrite accompanied by illite and inclusion-free-quartz. Optical microscopy, transmitted light.

Rhodochrosite 1

Rhodochrosite 1 occurs as anhedral inclusions in Fe-Kutnohorite-1, due to its scale we were unable to detect it in Optical microscopy.

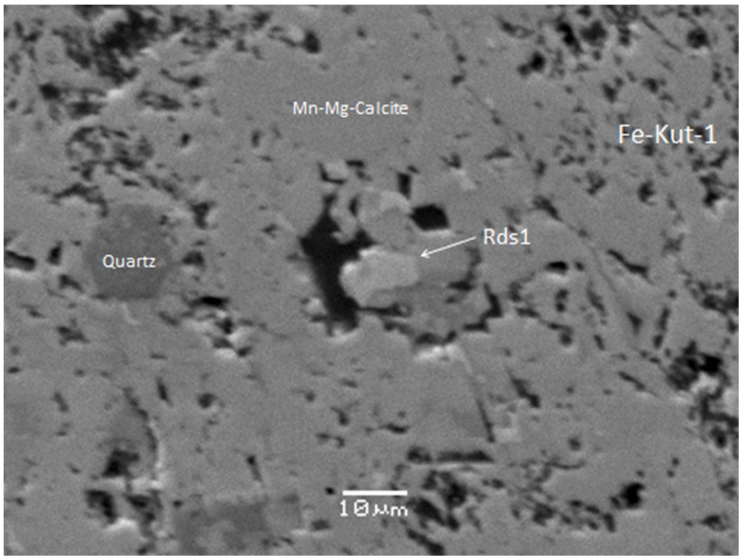

Fig. 26. Rds1=Rhodochrosite 1, Fe-Kut-1=Fe-kutnohorite-1. Rhodochrosite 1 grain hosted in Fe-kutnohorite-1 and Mn-Mg-calcite. EDS-SEM analysis.

Fe-Kutnohorite-1

Fe-kutnohorite-1 is highly porous and hosts anhedral rhodochrosite 1 inclusions as well as post-ore rhodochrosite 2 grains and veinlets. The anhedral rhodochrosite 1 inclusions within Fe-kutnohorite 1 are indicative that rhodochrosite 1 is a product of replacement process (Putnis, 2002). Fe-kutnohorite-1 and (Mn-Fe)-Mg-rich calcite have irregular grain boundaries, which combined with the presence of rhodochrosite 1 inclusions and porosity in Fe-kutnohorite-1, strongly suggest that Fe-kutnohorite 1 and rhodochrosite 1 are secondary hydrothermal Mn carbonates that were formed by carbonization of the wall rock (Mn-Fe)-Mg-rich calcite aided by Coupled Dissolution-Reprecipitation (CDR) reactions (Figure 26, 28) (Putnis, 2002; Putnis, 2009, M.Sc. Thesis M. Tzani, 2021).

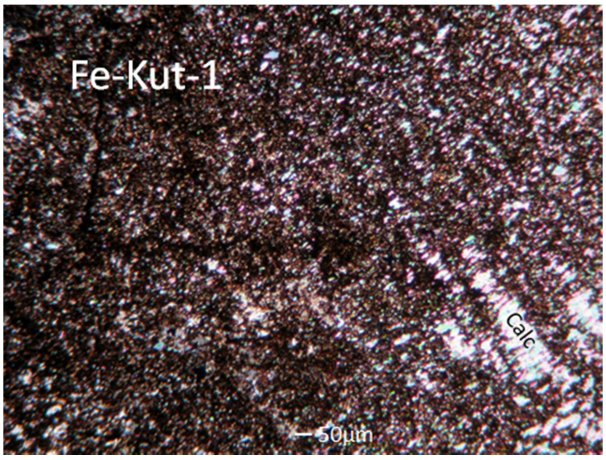

Fig. 27. Fe-Kut-1=Fe-Kutnohorite-1. Fe-kutnohorite-1 and calcite in optical microscopy with transmitted light.

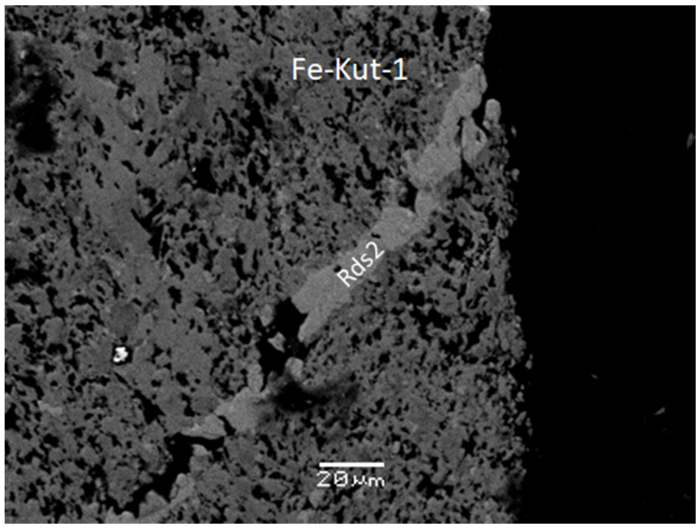

Fig. 28. Rds2=Rhodochrosite 2, Fe-Kut-1=Fe-Kutnohorite 1. Post-ore Rhodochrosite 2 vein crosscutting main-ore Fe-Kutnohorite 1. EDS-SEM analysis.

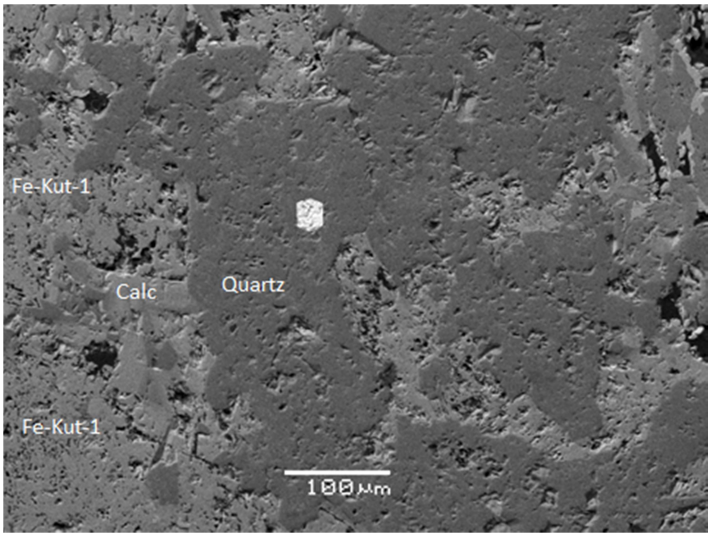

Fig. 29. Pyrite grain in quartz surrounded by calcite (Calc) and Fe-kutnohorite-1 (Fe-Kut-1). EDS-SEM analysis.

Kutnohorite 2

Kutnohorite 2 occurs as abundant rounded, elongated of irregular inclusions, with a size of <10 µm, hosted by jasperoid quartz, (M.Sc. M. Tzani 2021), indicating replacement of kutnohorite by quartz (Lovering, 1972; Cline 2001).

Minor rutile appears to crosscut the pre-ore stage pyrite, surrounded by quartz (Figures 30, 31 32 and 33). Rutile when disseminated can be surrounded by illite. (Figure 23 picture A, 32 pictures C-D and 33). This Rutile-Illite association may have resulted from alteration of the primary wall rock clinopyroxene (Diopside) by the ore fluids (Su et al., 2018).

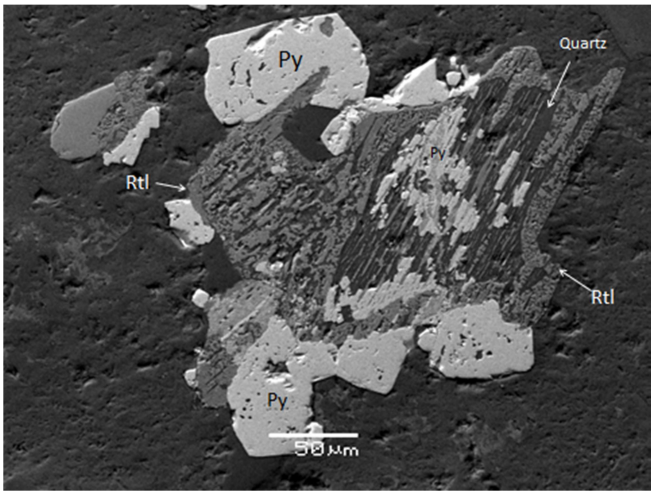

Fig. 30. Rtl=rutile, Py=pyrite. Pyrite and rutile in quartz-illite matrix. EDS-SEM analysis.

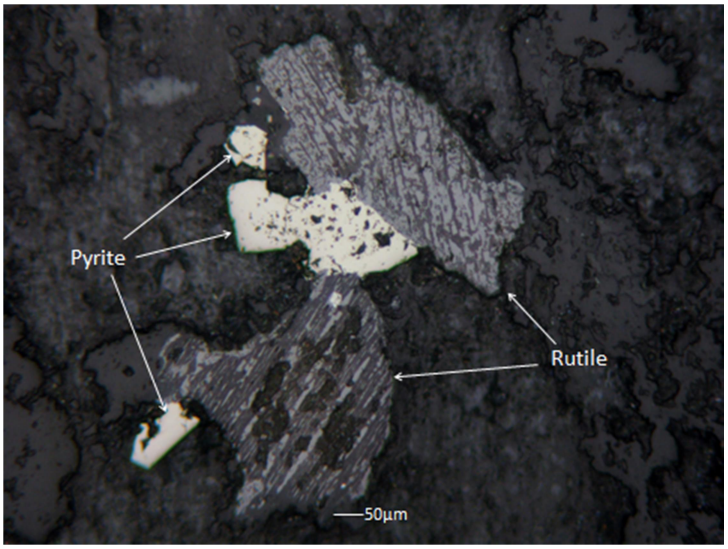

Fig. 31. Rutile grains crosscutting pyrite in quartz-illite matrix. Optical microscopy, reflected light.

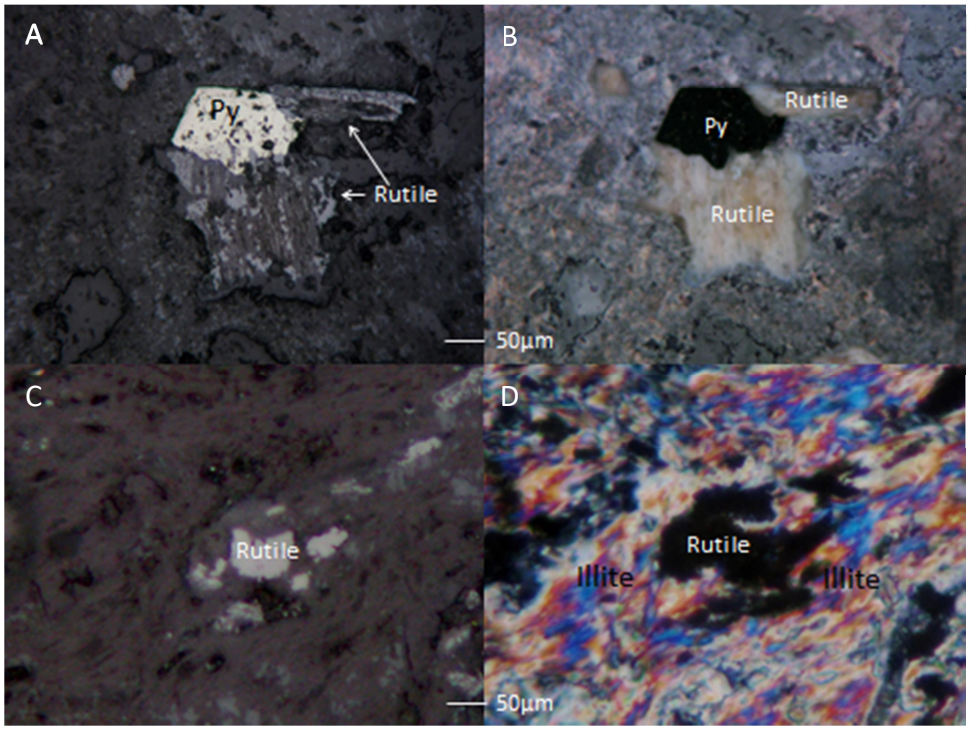

Fig. 32. Py=Pyrite. A-B pictures: Rutile grains crosscutting pyrite. C-D pictures: Rutile surrounded by illite. Optical microscopy reflected and transmitted light.

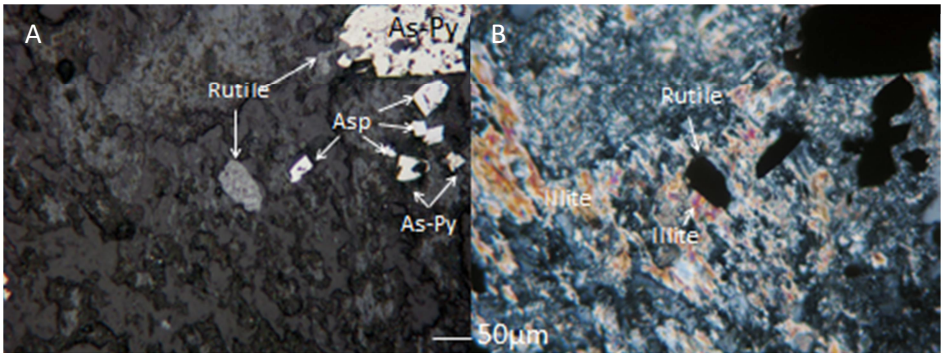

Fig. 33. A-B: Rutile within illite and quartz. Optical microscopy reflected and transmitted light.

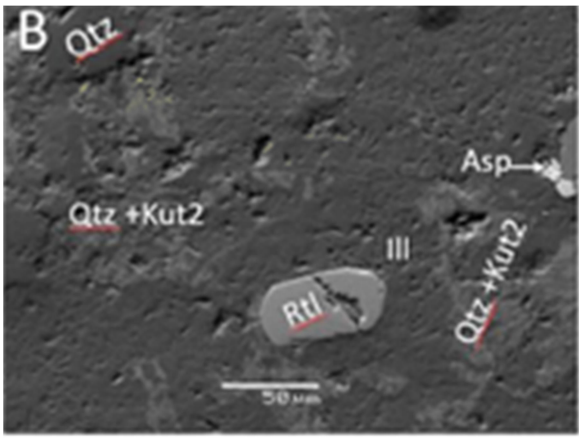

Fig. 34. EDS-SEM picture and description from Marina Tzani M. Sc. thesis, for comparison.
B: Rutile in association with illite and arsenopyrite, occur disseminated within the jasperoid quartz with kutnohorite 2 inclusions. The deposition of rutile during silicification implies that the fluid was moderately acidic (Thompson et al., 2004).

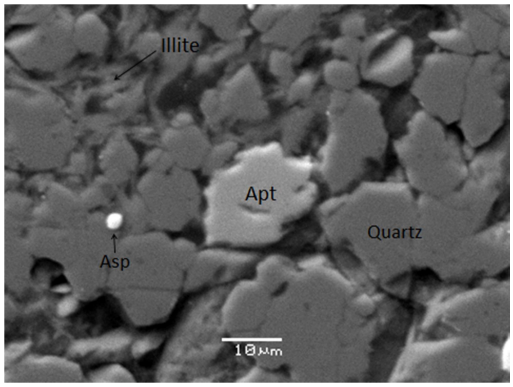

Fig. 35. Apt=Apatite, Asp=Arsenopyrite. Minor apatite in main ore stage. EDS-SEM. (M.Tzani, 2021)

Quartz in main ore stage has irregular shape, is fine grained and when accompanying As-pyrite and arsenopyrite, quartz is inclusion free. (Figures 24 picture B and 25). Calcite in the main-ore stage has varying Mg, Mn and Fe concentrations, specifically the concentration of Fe in main-

ore stage calcite is minimized due to carbonate dissolution (decarbonatization) of the primary wall rock calcite triggering Fe mobilization from the primary wall rock calcite. In SEM analysis Mg-rich calcite has a darker color. (Figure 36).

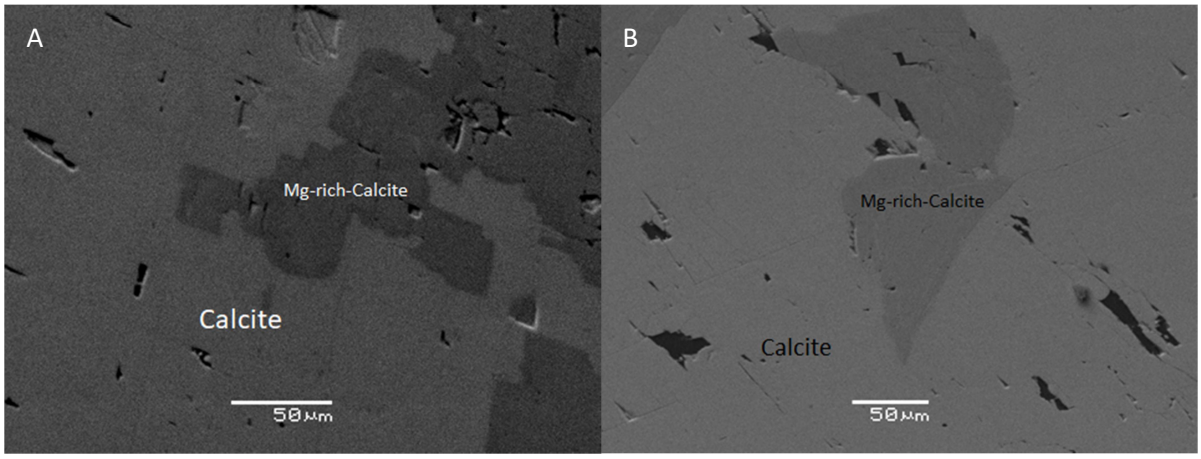

Fig. 36. A-B: Mg-rich-calcite and calcite. EDS-SEM analysis.

Post-Ore Minerals

Post-ore stage is identified by the presents of rhodochrosite 2. Rhodochrosite 2 is outlining and crosscutting main ore stage minerals. Figures 28, 37 and 38. The presents of Mn-poor calcite near rhodochrosite 2 indicates the mobilization of Mn from Calcite to form rhodochrosite 2 during post-ore carbonatization.

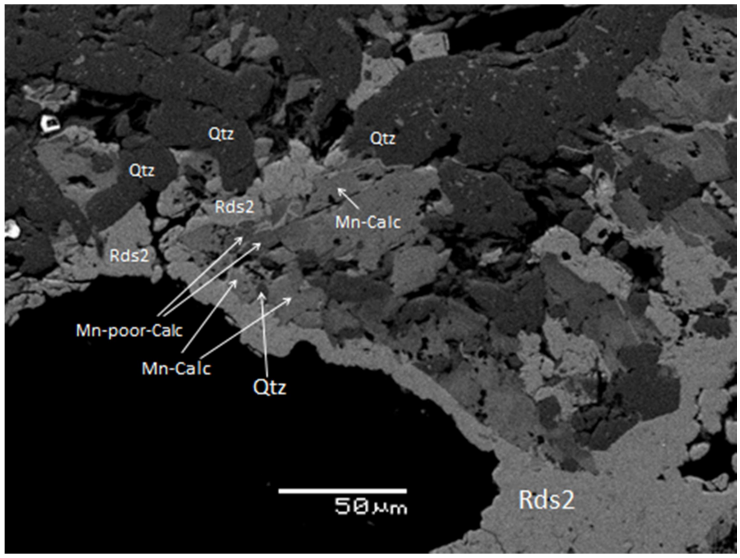

Fig. 37. Rds2=rhodochrosite 2, Qtz=quartz, Mn-Calc=Mn-calcite. Rhodochrosite 2 vein outlining and crosscutting calcite and quartz. EDS-SEM analysis.

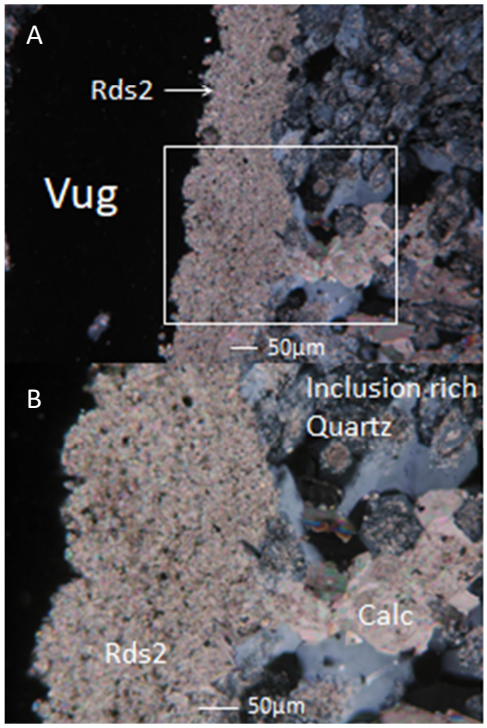

Fig. 38. Rds2=rhodochrosite 2, Calc=calcite. A-B: Rhodochrosite 2 outlining calcite and quartz-rich in calcite inclusions. Optical microscopy, transmitted light.

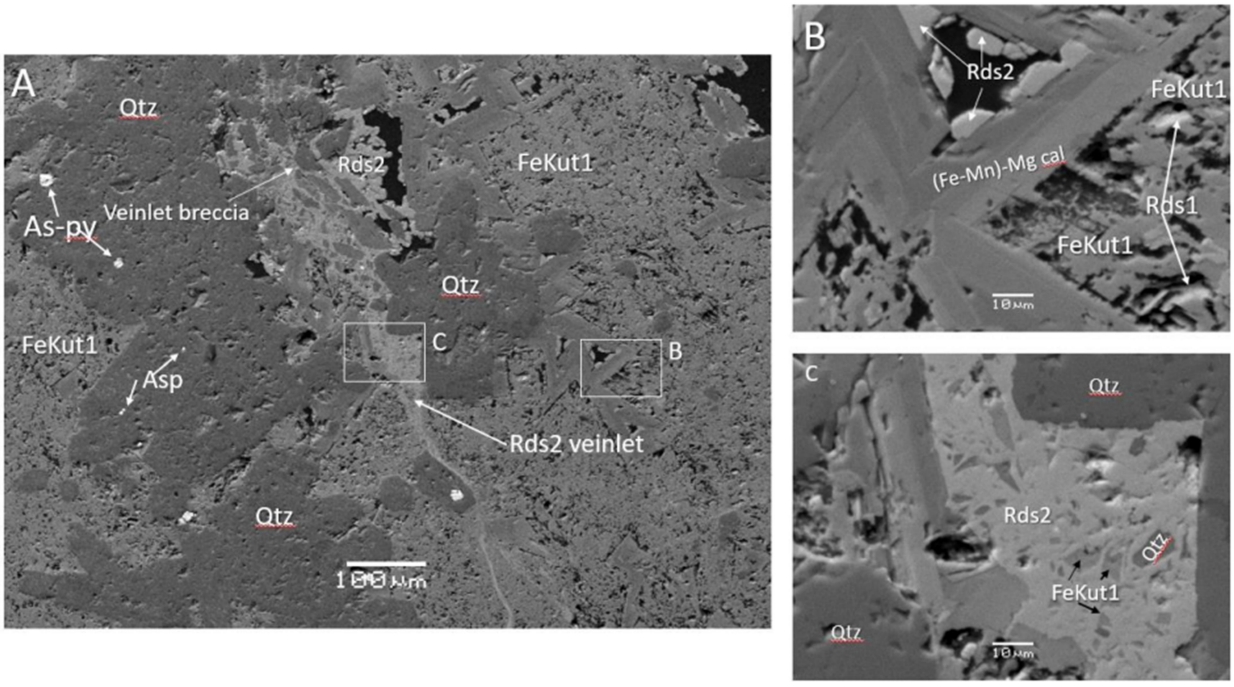

Fig. 39. EDS-SEM pictures and description from Marina Tzani M. Sc. thesis, for comparison.

Secondary electron-backscattered (SEM-BSE) images of main-ore and post-ore stages, wall rock alteration, silicification, and Mn carbonate and sulfide mineralization textures, and their paragenetic relationships, for the samples used in this study, Piavitsa Au deposit. Main-ore stage silicification (jasperoid quartz) (A), sulfidation (arsenopyrite, arsenian pyrite) (A),

carbonatization of wall rock calcite (kutnohorite 1, rhodochrosite 1) (B), and post-ore stage rhodochrosite 2 veinlets with local veinlet breccia that crosscut main-ore stage minerals (C), and vug-lining drusy rhodochrosite 2. (M.Sc. M. Tzani 2021).

Mineral Paragenesis

The following mineral paragenesis can be assumed based on the observations from the Optical and Scanning Electron Microscopy examination of the before mentioned samples. Calcite is the PRIMARY mineral phase as it is the main mineral of the unaltered carbonate host rocks. The first stage of hydrothermal alteration can be characterized by silicification of the carboniferous basement. This can be supported by synchronous decarbonization and the precipitation of euhedral and jasperoid quartz. These two quartz phases are related to a silicification stage that precipitates pyrite, galena, sphalerite, chalcopyrite and Cu-Pb-Sb-sulfosalts. A later argillic alteration is characterized by the presence of illite. Illite cross-cut quartz and is closely related with As-pyrite and Arsenopyrite, indicating that argillization of the silica's is related with the deposition of the As and Au in the ore stage. Present, with the argillic alteration and the ore bearing sulfides, are Mn-carbonate minerals such as kutnohorite and rhodochrosite.

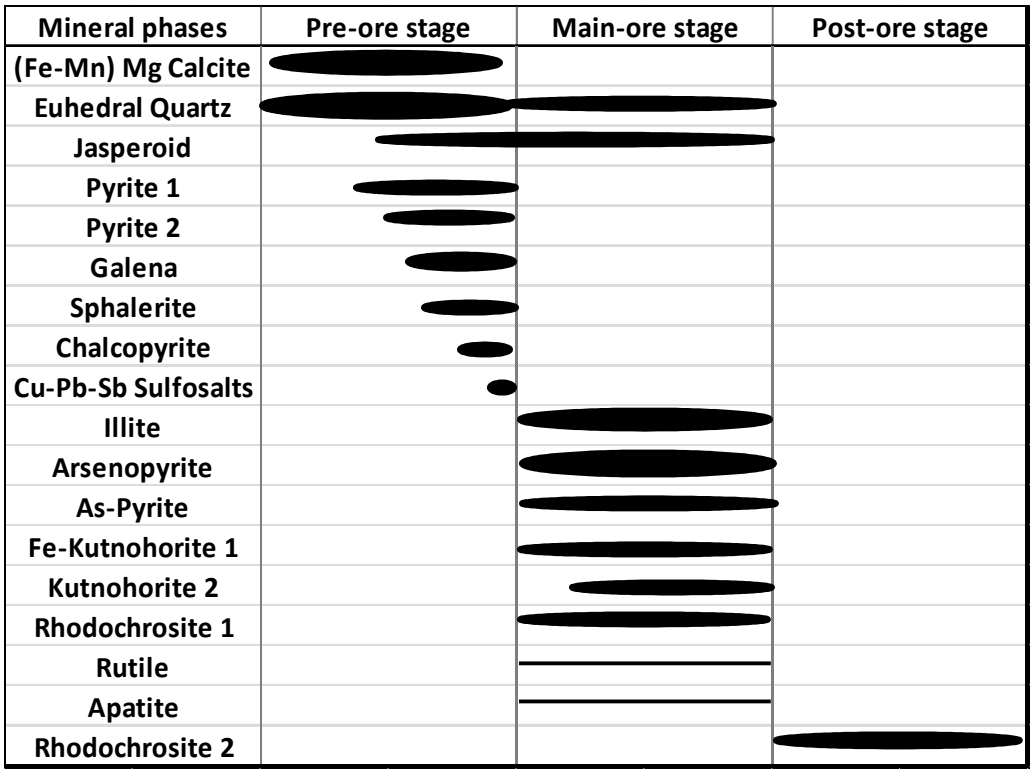

Fig 40: Simplified mineral paragenesis of Piavitsa Au-deposit. (Modified by Tzani 2021.)

Ore bearing minerals: Arsenopyrite and As-pyrite

The Au in Piavitsa deposit is largely ''invisible'' or ''refractory'', meaning that it is very difficult to detect by reflected light and scanning electron microscopy. The uncommon presence of free Au cannot be excluded, however, it needs to be verified. Arsenopyrite and Arsenian pyrite are the main hosts for As in the mineralized rock samples. The strong correlation between As and Au indicates that Au in Piavitsa is hosted in Arsenopyrite and As-pyrite. The presences of gold-bearing pyrite and/or marcasite in jasperoid formed by fluid-rock reaction are consistent with gold deposition during sulfidation of reactive iron in the host rocks (Cline, 2001). Geochemical relationship strongly suggests that Au is strongly associated with As: Pearson correlation coefficient values for Au and As (r=0.905; p-value=0.000) confirm what is apparent from the binary correlation plot that exhibit a clear strong positive correlation between As vs Au (R^2=0.812) (Fig. 41) moreover, cluster dendrograms also showed Au to be clustering with As with similarity >95% (Figure 42) (M.Sc. M. Tzani 2021).

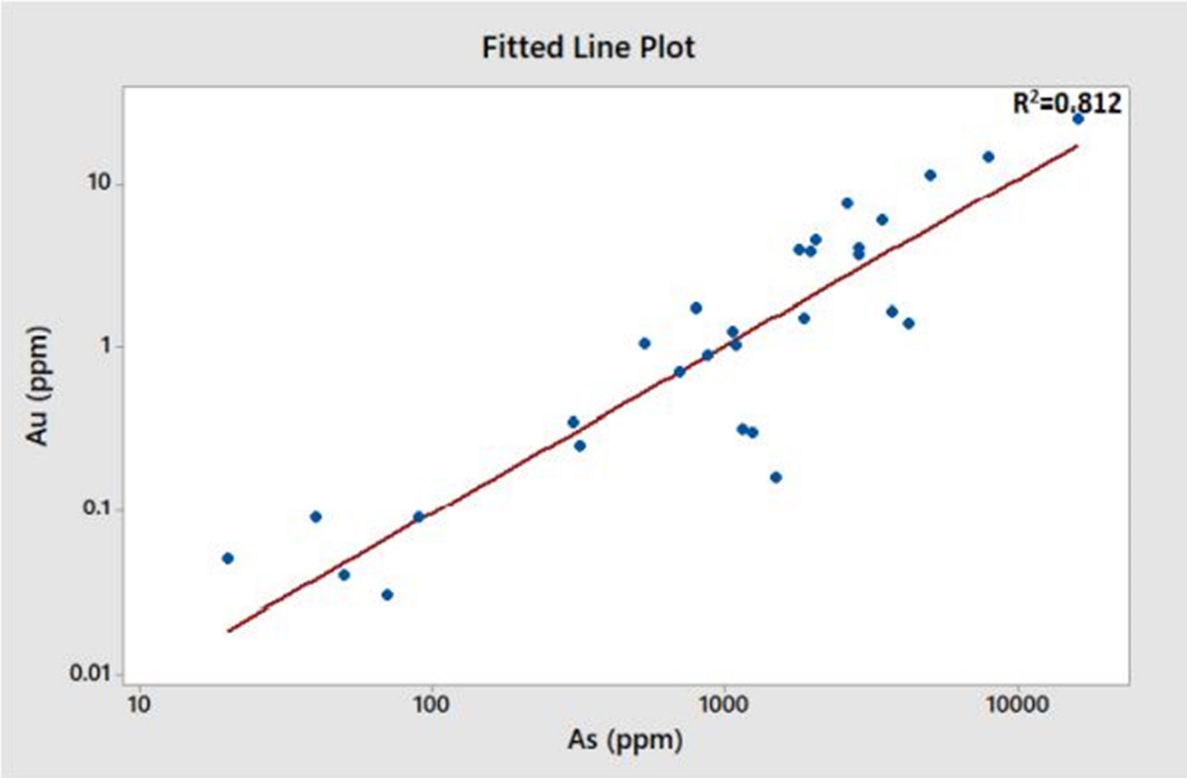

Fig. Fig. 41. Correlation plot of Au vs As of ore samples. (M.Sc. M. Tzani 2021)

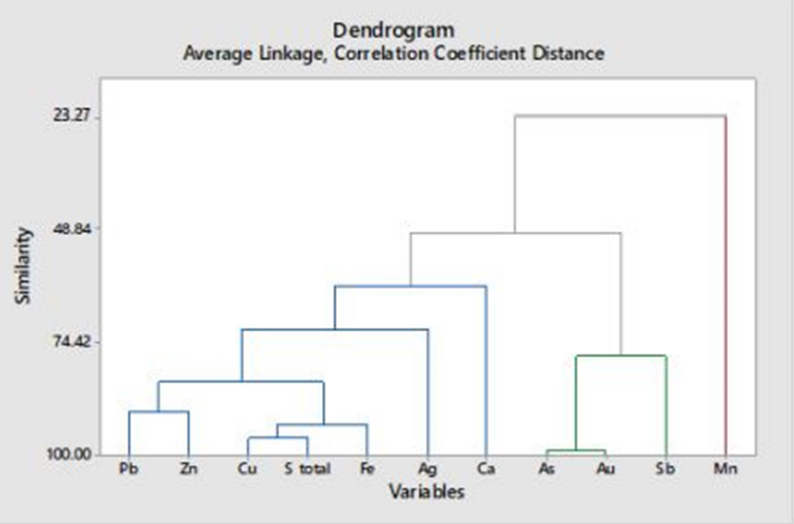

	Variables
Cluster 1	Pb Cu Zn Fe Ca Ag S
Cluster 2	As Sb Au
Cluster 3	Mn

Fig. 42. Dendrogram of ore samples with the 3 main clusters: Cluster 1, has Pb, Zn, Cu, S, Fe, Ag, and Ca and Cluster 2 has As, Au and Sb, as its members, respectively, whereas Cluster 3 has Mn as its only member. Cluster 1 is divided into two subgroups, with Pb, Cu, Zn, Fe, Ag, and S in the first subgroup, and Ca in the second. Cluster analysis has shown that Au is clustering with As with > 98% similarity and with Sb with > 75% similarity. (M.Sc. M. Tzani 2021)

Discussion

Piavitsa gold deposit has hybrid characteristics between Carlin type deposits and carbonate replacement deposits. Carlin type deposits are enriched in As-Sb-Hg-Tl, while carbonate replacement deposits are enriched in As-Sb-Pb-Zn ± Ag, Mn, Tl, Te, Cu, Hg, Bi and Sn (Thompson et al, 2004). These are the most crucial evidences we have that support the hybrid characteristics:

Carlin type deposits:

1) The dominant sulfide mineral assemblage in Carlin type deposits includes arsenian pyrite, arsenopyrite, realgar and orpiment and the deposits are characterized by the As-Sb-Hg-Tl association (Thompson et al, 2004).
2) In Carlin type deposits gold occurs as thin films coating arsenian pyrite, submicron-sized inclusions of native Au in arsenian pyrite and as structurally bound atoms of Au in arsenian pyrite (Hofstra & Cline, 2000)
3) The evidence of sulfidation of host-rock Fe (Hofstra & Cline, 2000)

Carbonate-replacement deposits:

1) Au-rich carbonate-replacement deposits form the most distal member of the sequence of intrusion-related deposits in zoned intrusions centered camps (Sillitoe & Bonham, 1990). Just like in Kassandra mining district.
2) Carbonate-replacement deposits are part of a family of deposits zoned around magmatic-hydrothermal, intrusion-centered systems that include porphyry, skarn and vein deposits (Sillitoe, 1991a).

Conclusion

The key mineralogical features of the Piavitsa Au deposit match the features that M. Tzani described in her thesis and include the following:

1) Pre-ore stage minerals are: (Mn-Fe)-Mg calcite, jasperoid and euhedral quartz, galena, As-poor-pyrite, sphalerite, Cu-Pb-Sb-sulfosalts, chalcopyrite and Fe-oxides. Main-ore stage minerals are: Arsenopyrite, As-pyrite, Fe-kutnohorite 1, rhodochrosite 1, kutnohorite 2, illite, rutile and apatite. Post-ore stage mineral: Rhodochrosite 2.
2) Pre-ore stage alterations are: Decarbonatization, silicification and sulfidation. Main-ore stage alterations are: Silicification, argillization, carbonatization and sulfidation. Post-ore stage alterations are: Carbonatization.

Future Research

The nature of Au in arsenopyrite and Arsenian-pyrite is yet to be determined. Therefore we suggest the use of LA-ICP-MS to address this mater. Also the use of LA-ICP-MS in presumable gold-bearing arsenopyrite and Arsenian-pyrite can create chemical map analysis for trace elements such as Sb, Hg, Tl, Ag, Mo, Te, Se, Bi and V. This will also further clarify the already stated relation between Sb-Au. (See ‘’Ore bearing Minerals’’). LA-ICP-MS imaging technique, which enables a suite of trace elements to be simultaneously measured across the surface of pyrite grains. The low detection limit and simultaneous capture of data for up to 20 trace elements make this a powerful analytical tool for understanding pyrite genesis and evolution. This technology allows the mapping of both invisible gold and gold particles within pyrite and thus a comparison of gold distribution with the pyrite texture and the zoning of the trace elements in the pyrite (Large et al, 2009).

References

1) Albert H. Hofstra & Jean S. Cline. ''Characteristics and Models for Carlin-Type Gold Deposits'', SEG Reviews, Vol. 13, 2000, p. 163-220.

2) Siron, C. R., Thompson, J. F., Baker, T. R., Darling, R. S., & Dipple, G. M. (2019). ''Origin of Au-Rich Carbonate-Hosted Replacement Deposits of the Kassandra Mining District, Northern Greece: Evidence for Late Oligocene, Structurally Controlled, and Zoned Hydrothermal Systems''. Economic Geology, 114(7), 1389-1414.

3) C. R. Siron, John F.H. Thompson, Tim Baker, Richard Friedman, Pavlos Tsitsanis, Sally Russell, Scott Randall, and Jim Mortensen. ''Magmatic and Metallogenic Framework of Au-Cu Porphyry and Polymetallic Carbonate Hosted Replacement Deposits of the Kassandra Mining District, Northern Greece''. 2016 SEG, Inc. Special Publication 19, pp 29-55 .

4) Marina Tzani, M.Sc. Thesis 2021. ''Coupling between mineral replacement reactions and co-precipitation of invisible gold and arsenic in the Piavitsa carbonate-replacement gold deposit, Kassandra Mining District, N. Greece''.

5) W. Su, W. Dong, X. Zhang, N. Shen, R. Hu, A. H. Hofstra, L. Cheng, Y. Xia and K. Yang. (2018). ''Carlin-Type Gold Deposits in the Dian-Qian-Gui ''Golden Triangle'' of Southwest China''. 2018 SEG, Inc. Reviews in Economic Geology, v. 20, pp 157-185.

6) Eldorado gold, June 27, 2021. Eldorado Gold Corporation Exploration Update.

7) Eldorado gold, December 15, 2021. Eldorado Gold Releases Updated Mineral Reserve and Mineral Resource Statement.

8) Eldorado gold, October 23, 2014. Eldorado Gold Announces Drilling Update.

9) Jean S. Cline. (2001). ''Timing of Gold and Arsenic Sulfide Mineral Deposition at the Getchell Carlin-Type Gold Deposit, North-Central Nevada''. Economic Geology vol. 96, 2001, pp. 75-89.

10) R. R. Large, L. Denyushevsky, C. Hollit, V. Maslennikov, S. Meffre, S. Gilbert, S. Bull, R. Scott, P. Emsbo, H. Thomas, B. Singh and J. Foster. ''Gold and Trace Element Zonation in Pyrite Using a Laser Imaging Technique: Implications for the Timing of Gold in Orogenic and Carlin-Style Sediment-Hosted Deposits''.

11) J. F. H. Thompson, V. G. Gale, R. M. Tosdal and W. A. Wright. ''Characteristics and Formation of the Jeronimo Carbonate-Replacement Gold Deposit, Potrerillos District, Chile''. 2004 Society of Economic Geologist, Special publication 11, 2004, pp.75-95.

12) A. Putnis, Mineralogical Magazine, October 2002 ''Mineral replacement reactions: from macroscopic observations to microscopic mechanisms''.

13) A. Putnis, Reviews in Mineralogy & Geochemistry, 2009 ''Mineral Replacement Reactions''.

14) Kesler, S.E., Riciputi, L.C., Ye, Z.J., 2005. ''Evidence for a magmatic origin for Carlin-type gold deposits: isotopic composition of sulfur in the Betze-Screamer deposit, Nevada, USA''.

15) Zhuo-Jun Xie, Y. Xia, J. S. Cline, Bao-Wen Yan, Ze-Peng Wang, Qin-Ping Tan, Dong Tian Wei, 2016,. ''Comparison of the native antimony-bearing Paiting gold deposit, Guizhou Province, China, with Carlin-type gold deposits, Nevada, USA''.

16) D.P. Stenger, S.E. Kesler, D.R. Peltonen and C.J. Tapper, 1998. ''Deposition of Gold in Carlin-Type Deposits: The Role of Sulfidation and Decarbonation at Twin Creek, Nevada'' Economic Geology Vol. 93, 1998, pp. 201-215.

17) I. B. Butler, D. Rickard, 2000. ''Framboidal pyrite formation via the oxidation of iron (II) monosulfide by hydrogen sulphide''. Volume 64, Issue 15, August 2000, Pages 2665-2672.

18) Δημήτρης Ι. Παπανικολάου, Γεωλογια της Ελλάδας.

19) Christensen, O.D., 1995, Carlin Trend geologic overview: Society of Economic Geologists Guidebook Series, v. 8, p. 12–26.

20) Sillitoe, R.H., 1991a, Intrusion-related gold deposits, in Foster, R.P., ed., Gold metallogeny and exploration: Glasgow, Blackie and Son, p. 165–209. 1991b, Gold metallogeny in Chilean introduction: Economic Geology, v. 86, p. 1187–120.

21) Albino, G.V., 1995, Porphyry copper deposits of the Great Basin-Nevada, Utah and adjacent California: Arizona Geological Society Digest 20, p. 267–296.

22) Eldorado gold, June 27, 2012 ''Eldorado Gold Corporation Exploration Update''.